



**Miguel Pedro da Conceição Monteiro**

Bachelor of Science in Micro and Nanotechnologies Engineering

**Flexible sensors technology for Point-Of-Care  
diagnostics with integrated micro fluidics on paper**

Dissertation submitted in partial fulfilment of the  
requirements for the degree of

Master of Science in  
**Micro and Nanotechnologies Engineering**

Supervisor: Dr. Luigi G. Occhipinti, Professor,  
Department of Engineering, University of Cambridge

Co-Supervisor: Dr. Luís Miguel Nunes Pereira, Assistant Professor,  
Faculdade de Ciências e Tecnologia da Universidade Nova de Lisboa

Examination Committee

Chairperson: Dr. Rodrigo Ferrão de Paiva Martins, Full Professor, FCT-UNL

Raporteurs: Dr. Rui Alberto Garção Barreira do Nascimento Igreja, Assistant Professor, FCT-UNL

Dr. Luís Miguel Nunes Pereira, Assistant Professor, FCT-UNL



FACULDADE DE  
CIÊNCIAS E TECNOLOGIA  
UNIVERSIDADE NOVA DE LISBOA

**September, 2018**

**Flexible sensors technology for Point-Of-Care diagnostics with integrated micro fluidics on paper**

Copyright © Miguel Pedro da Conceição Monteiro, Faculdade de Ciências e Tecnologia, Universidade Nova de Lisboa.

The Faculty of Sciences and Technology e a NOVA University of Lisbon holds the right, forever and without geographical limitations, to file and publish this dissertation through printed copies reproduced on paper or in digital form, or by any other means known or to be disclosed, and to disseminate it through repositories and to allow them to be copied and distributed for non-commercial educational or research purposes, provided the author and publisher are given credit.

# **Acknowledgements**

First of all, I would like to express my appreciation for the excellent work developed by Professor Elvira Fortunato and Professor Rodrigo Martins for their significant contribute in the recognition of the NOVA University of Lisbon among the scientific community.

I would like to take this opportunity to express my gratitude to my institution, the Faculty of Sciences and Technology of the NOVA University of Lisbon, to the department of Materials Science for the possibility to develop this master thesis project in coordination with such a renowned institution as the University of Cambridge.

Such important projects as BET-EU are only possible when two great institution come together and work in a partnership. I will be always grateful for the opportunity to work in this project.

This was, without a doubt, an outstanding challenge both as a person and as a professional and I will be always very thankful to everyone that supported me along these months of hard work.

In the University of Cambridge, I had the privilege to work in collaboration with Professor Luigi Occhipinti, who always helped me with new ideas and the best work conditions. I am very grateful for his commitment to this project.

I would also like to express my sincere thanks to Professor Luís Pereira as well, for being an important piece in the bridge between both universities.

For its help in a crucial moment of this work I want to thank Professor João Fernandes.

To my colleagues in the University of Cambridge Pelumi Oluwasanya, Dr. Xiang Cheng, Dr. Varindra Kumar, Edward Tan, Jason Deacon, Lorenzo Pedrazzetti, Lucia Lombardi and Giuditta Stevanato for welcoming me, in a new city, for their excellent cooperation and for all the knowledge they shared with me. I want to thank as well to Carolina Marques, Ines Cunha, Paul Grey, Cristina Gaspar and Jonas Deurmeier for all the help and patience.

I could never forget to thank to all my colleagues in the course of Micro and Nanotechnology, that accompanied me for all these years and that I had the pleasure to work with. To my deepest friends Pedro Trigo, José Correia, Tomás Vasconcelos, Nuno Bártolo, Luka Lett, Bernardo Mendes, Marco Moreira, Sofia Martins and José Rui for all the life experiences that I will never forget. The jokes, the parties and the laughs we shared is something that will be with me forever.

As to my friends, João Silva, João Antunes Silva, Nuno Lobo and André Pereira for the support they gave me all the way here and, without them, it would not be possible.

Finally, but not the least, to my whole family which supported me, the sacrifices they did to make this possible, the motivation they provided me in all my projects and dreams and for making me the person I am today, I want to send my deepest gratitude.

## ***Abstract***

Nowadays the hospitals and the medical centres face a huge challenge finding solutions to improve the efficiency of medical diagnosis.

The scope of this project was to develop a “Point-of-Care Diagnostic” (POCD) device, that can give a better alternative for genetic analysis, instead of the usual methods of PCR (polymerase chain reaction).

This device is composed by three layers. The first layer which works as a transporter and filter was built on paper. The second layer is the substitute of the regular thermocycling phase in the PCR technique and the third layer incorporates an interdigital capacitor that works as a DNA (deoxyribonucleic acid) sensor with high sensitivity to detect DNA hybridisation. These last two layers were made in kapton film.

The devices were produced with microfabrication methods using inkjet printing, lithographic and deposition processes.

The device’s characterisation was based on impedance spectroscopy methods.

With the purpose of testing the device, the capacitor was functionalised with the YWHAZ gene. However, this process can be performed with any other gene.

Due to its characteristics, the device under study was designed to run RT-qPCR (Real time quantitative polymerase chain reaction) and presents itself as an effective way to substitute the traditional PCR techniques. Even more, as the transport of samples to a laboratory and the recruitment of specialised personnel are not necessary, costs and response time are reduced.

**Keywords:** POCD, RT-qPCR, bioelectrical read out, microfluidics on paper, biosensors, microheaters.

## Resumo

Um dos grandes desafios que os serviços de saúde enfrentam nos nossos dias é encontrar métodos de diagnóstico acessíveis e que permitam obter resultados fiáveis de forma rápida e eficaz.

Neste trabalho apresentamos um protótipo de um dispositivo de *Point-of-Care Diagnostic* (POCD) que possa substituir as técnicas tradicionais de PCR (*polymerase chain reaction*) que são atualmente usadas nos testes genéticos.

O dispositivo em análise é composto por três camadas. A primeira camada funciona como transportador e filtro da amostra e foi fabricada em papel. A segunda camada tem a função de substituir o habitual processo de *thermocycling* na técnica de PCR e a terceira camada incorpora um condensador interdigital que funciona como sensor de DNA (*deoxyribonucleic acid*) com elevada sensibilidade e que irá detetar a hibridização do DNA. Estas duas últimas camadas foram feitas em *kapton film*.

Estas camadas foram obtidas através de métodos de microfabricação, utilizando designadamente *inkjet printing*, processos litográficos e de deposição.

A caracterização dos dispositivos foi obtida utilizando métodos de espectroscopia de impedância.

Para testar o dispositivo, o condensador foi funcionalizado com o gene YWHAZ. No entanto, este processo pode ser realizado com qualquer outro gene.

Deste modo, o dispositivo em estudo pretende efetuar a leitura de RT-qPCR (*Real time quantitative polymerase chain reaction*) apresentando-se como uma alternativa aos atuais métodos laboratoriais, uma vez que não implica a necessidade de transportar as amostras a um laboratório, minimizando custos de transporte e tempo de resposta.

**Palavras-chave:** POCD, RT-qPCR, leitura bio eletrónica, microfluídica em papel, biossensores, microresistencias.

# Contents

List of Figures .....	viii
List of Tables .....	x
Symbols .....	xi
Acronyms .....	xii
Motivation and Objectives .....	xiii
<b>1. Introduction .....</b>	<b>1</b>
<b>1.1. RT-QPCR .....</b>	<b>3</b>
<b>1.2. CAPACITIVE SENSOR .....</b>	<b>4</b>
1.2.1. IMPEDANCE .....	6
1.2.1.1. ELECTRONIC MODEL .....	6
1.2.1.2. ELECTRICAL DOUBLE LAYER .....	7
<b>1.3. MICROHEATERS AND HEAT SENSORS .....</b>	<b>8</b>
<b>1.4. MICROFLUIDICS .....</b>	<b>8</b>
<b>2. Methodology .....</b>	<b>9</b>
<b>2.1. OVERALL VIEW OF LAYERS OF THE DEVICE AND THE SETUP .....</b>	<b>9</b>
<b>2.2. MICROFLUIDIC PROCESS .....</b>	<b>9</b>
<b>2.3. CONTACT ANGLE TECHNIQUE .....</b>	<b>10</b>
<b>2.4. FABRICATION .....</b>	<b>11</b>
2.4.1. PHOTOLITHOGRAPHY WITH AZ PHOTORESIST .....	11
2.4.2. METALLIZATION PROCESS .....	12
2.4.3. SU8 WELL .....	12
<b>2.5. CHARACTERISATION .....</b>	<b>13</b>
2.5.1. IMPEDANCE SPECTROSCOPY .....	13
<b>2.6. FUNCTIONALISATION OF THE CAPACITOR .....</b>	<b>13</b>
2.6.1. CLEANING STEP .....	14
2.6.2. PREPARATION AND FUNCTIONALISATION .....	14
2.6.3. RINSING PROCESS .....	14
<b>2.7. HYBRIDISATION STUDIES .....</b>	<b>14</b>
<b>2.8. RT-QPCR PROCESS .....</b>	<b>15</b>
2.8.1. THERMOCYCLING .....	16
<b>2.9. X-RAY PHOTOELECTRON SPECTROMETER .....</b>	<b>16</b>
<b>3. Analysis of Results .....</b>	<b>17</b>
<b>3.1. MICROFLUIDICS .....</b>	<b>17</b>
<b>3.2. RESISTANCE /HEAT .....</b>	<b>19</b>
<b>3.3. IMPEDANCE .....</b>	<b>22</b>
<b>3.4. X-RAY PHOTOELECTRON SPECTROSCOPY (XPS) .....</b>	<b>24</b>
<b>4. Conclusion .....</b>	<b>29</b>

<b>5. Future perspectives .....</b>	<b>30</b>
<b>References and Bibliography.....</b>	<b>31</b>
<b>Appendix.....</b>	<b>35</b>

## List of Figures

FIGURE 1 SCHEME OF THE SENSOR.....	2
FIGURE 2 A) SHOWS THEORETICALLY THE TYPE OF RESPONSE THAT WE WILL OBTAIN WITH AN OPTICAL RT-PCR; B) ONE CYCLE OF PCR; C) THERMOCYCLER GRAPHIC; D) SCHEMATIC OF AN EXAMPLE OF FLUORESCENT ASSAY TAQMAN PROBE QPCR .....	4
FIGURE 3 SCHEMATIC OF SENSOR. ....	5
FIGURE 4 BEHAVIOUR OF EACH COMPONENT IN THE NYQUIST PLOT. ....	6
FIGURE 5 A) CROSS SECTION OF EIS WITH ELECTRIC EQUIVALENT CIRCUIT B) SCHEMATIC OF THE TOP VIEW AND FEATURES .....	7
FIGURE 6 THE DIFFERENT LAYERS OF THE DEVICE.....	9
FIGURE 7 A) INKJET DIMATIX 5200; B) WAVEFORM FOR EMD6415; C) SETUP USED TO FABRICATE MICROFLUIDICS .....	10
FIGURE 8 FTA 1000 ANALYSER SYSTEM .....	11
FIGURE 9 A) LASER WRITER; B) MASK ALIGNER - MA/BA; C) PHOTOLITHOGRAPHIC PROCESS.....	12
FIGURE 10 CASCADE PROBE STATION. ....	13
FIGURE 11 THE RELATION BETWEEN THE HYBRIDISATION AND THE IMPEDANCE.....	15
FIGURE 12 DIMATIX JETTING AND DROPLET FORMATION A) DROP COMING OUT OF THE NOZZLE; B) JETTING OF THE DROPS .....	17
FIGURE 13 CONTACT ANGLE 20 LAYERS OF INK A) WHATMAN N°1; B) SUPOR PORE 200 BY PALL COMPANY .....	17
FIGURE 14 DESIGN AND FLUX TEST OF THE MICROFLUIDIC LAYER .....	18
FIGURE 15 SAMPLE OF WHATMAN N° 1 PORE SIZE 10 $\mu\text{M}$ - A) AND B); SUPOR PORE 200 PORE SIZE 0.2 $\mu\text{M}$ - C) AND D); SANDWICH ASSAY USING THE WHATMAN N°1 ON TOP AND THE SUPOR PORE 200 BELLOW – E) AND F) ...	19
FIGURE 16 A) RESISTANCE LAYER; B) RESISTANCE MEASURED IN THE CAPACITOR .....	20
FIGURE 17 EXAMPLE OF THE IV SWEEP TAKEN TO CHARACTERISE THE RESISTANCES .....	20
FIGURE 18 THERMO IMAGE OF THE RESISTANCES BEFORE AND AFTER APPLYING CURRENT THROUGH THE RESISTANCE A) ROOM TEMPERATURE; B) AFTER APPLYING CURRENT .....	21
FIGURE 19 THERMOCYCLER THE INCREASE OF TEMPERATURE FOR EACH CURRENT WITH AND ERROR OF 0.1° .....	21
FIGURE 20 DIFFERENT PLOTS OBTAINED BY IMPEDANCE SPECTROSCOPY .....	22
FIGURE 21 EQUIVALENT MODEL AND FITTING A) BODE DIAGRAM B) NYQUIST .....	23
FIGURE 22 SHOWS THE XPS SPECTRA OF EACH CHEMICAL ELEMENT WERE THE POINTS IN BLUE REPRESENT A SAMPLE FUNCTIONALIZED WITH SAM AND DS DNA AND THE GREEN POINTS IS A SAMPLE WHERE IT WAS REMOVED THE DNA WITH RESPECTIVE FITTING ADJUSTMENTS (N – NITROGEN, C – CARBON, S – SULFUR, P – PHOSPHOR, O – OXYGEN).....	25
FIGURE 23 NUCLEOTIDES STRUCTURE. ....	26
FIGURE 24 IN THIS IMAGE IT IS SHOWN THE DISTRIBUTION OF THE ELEMENTS IN SAMPLE.....	28
FIGURE 25 AZ PHOTORESIST WITH 5 $\mu\text{M}$ FEATURES AFTER DEVELOPMENT.....	35
FIGURE 26 CAPACITOR FEATURES TEST .....	36
FIGURE 27 SAMPLE OF KAPTON WITH 25 $\mu\text{M}$ .....	36



FIGURE 28 DEFECTS FOUND ON THE DEVICES AFTER THE FABRICATION STEP .....	37
FIGURE 29 JD MASK .....	37
FIGURE 30 A) TYPICAL BEHAVIOUR OF CAPACITOR WITH MAGNITUDE VS FREQUENCY A) LINEAR SCALE, B) LOG SCALE. ....	38
FIGURE 31 IMPEDANCE SPECTROSCOPY THROUGH THE THERMO CYCLING PROCESS A) MAGNITUDE, B) PHASE AND C) HOW THE IMPEDANCE CHANGES WITH N° O CYCLES FOR A FREQUENCY OF 55 MHZ.....	39
FIGURE 32 PRESENTED ABOVE IT IS THE PLOTE OF THE IMPEDANCE MAGNITUDE WITH FREQUENCY. A) AND B) IS THE PLOT OF THE SAMPLE TAKEN WHEN THE PROBES WERE WORKING AND SHOWING RESULTS ACCORDING WITH THE LITERATURE. C) AND D) IT IS THE PLOTE TAKEN A FEW DAYS AFTER WITH SAME CONDITION AND FROM THE PLOTE IT IS POSSIBLE TO NOTICE THAT SOME REGIONS OF THE GRAPHIC WHERE AFFECTED. E) AND F) IS A TESTE GRAPHIC MADE WITH THE SAME PARAMETERS BUT TO A SMD CAPACITOR WITH A FIXED VALUE OF CAPACITANCE 47pF.....	40
FIGURE 33 BODE DIAGRAM AND NYQUIST.....	41
FIGURE 34 THE COMPLETE SPECTRUM OBTAINED WITH XPS .....	42

## ***List of Tables***

TABLE I CONTENTS NECESSARY FOR A QPCR AS FOR THE RESPECTIVE VOLUMES .....	16
TABLE II ALL BLOOD COMPOSITION .....	18
TABLE III AVERAGE VALUES OF THE RESISTANCES PRESENTED IN FIGURE 16 .....	20
TABLE IV DISTRIBUTION AND CONCENTRATION OF ELEMENTS IN THE SAMPLES .....	26
TABLE V SHOWS A POSSIBLE DECOMPOSITION OF THE XPS SPECTRA WITH BINDING ENERGIES COLLECTED FROM THE GRAPHICS IN THE FIGURE 22 .....	26
TABLE VI CHEMICAL LIST .....	28

## Symbols

$A$	Area
$A_i$	Concentration of analyte $i$ .
$C$	Coulomb
$d$	Distance
$F$	Farad
$G$	distance between the electrodes
$Hz$	Hertz
$j$	Imaginary unit ( $\sqrt{-1}$ )
$l$	Length
$N_A$	Avogadro number
$Q$	Constant with dimension $F \cdot s \cdot n^{-1}$
$r$	Equivalent capillary pore radius of paper
$R$	Electrical resistance
$s$	Second
$t$	Time
$t_{EIS}$	Thickness of the interdigital electrodes
$W$	the size of the finger
$Z$	Electrical impedance
$\gamma$	Surface tension
$\gamma_{LG}$	Surface tension of the liquid-gas interfaces
$\gamma_{SG}$	Surface tension of the solid-gas interfaces
$\gamma_{SL}$	Surface tension of the solid-liquid interfaces
$\varepsilon$	Permittivity
$\varepsilon_0$	Permittivity in vacuum
$\eta_v$	Viscosity of the liquid
$\eta_s$	Sensor efficiency
$\theta_C$	Contact angle
$n$	Number of the fingers
$\omega$	Angular frequency

## Acronyms

3-MPA	3-Mercaptopropionic acid
AC	Alternating current
BE	Binding energy
bp	Base pair
BSA	Bovine serum albumin
cDNA	Complementary DNA
CPE	Constant phase element
cps	counts per second
Ct	Threshold cycle
<i>DI</i>	Deionized Water
DNA	Deoxyribonucleic acid
dNTP	Deoxynucleoside triphosphate
dsDNA	Double-stranded DNA
EDC	N-(3-Dimethylaminopropyl) - N'-ethylcarbodiimide hydrochloride
ELISA	enzyme-linked immunosorbent assay
FAM	6-carboxy-tetramethylrhodamine
GMO	Genetically modified organism
IDC	Interdigital capacitive
IDEs	Interdigitated electrodes
<i>IPA</i>	2-Propanol
LED	Light-emitting diode
LWR	Lucas-Washburn-Rideai
PBS	Phosphate buffer saline
PCR	Polymerase chain reaction
POCD	Point-of-Care diagnostic
POCT	Point-of-Care testing
Q-PCR	Quantitative polymerase chain reaction
RNA	Ribonucleic acid
RPM	Revolutions per minute
RT-PCR	Reverse transcription polymerase chain reaction
RT-qPCR	Real time quantitative polymerase chain reaction
SAM	Self-assembling monolayers
SCF	Spontaneous capillary flow
SPR	Surface plasmon resonance
SS-DNA	Single-stranded DNA
TAMRA	6-carboxy-tetramethylrhodamine
TM	Temperature of melting
UV	Ultraviolet
WLRS	White light reflectance spectroscopy
XPS	X-ray photoelectron spectroscopy
ZIF	Zero insertion force

## ***Motivation and Objectives***

This project was developed at the University of Cambridge, in collaboration with CENIMAT in the scope of the BET-EU European project. The main goal of this work was to produce a multilayer flexible label-free, biosensor for use in Point-of-Care diagnostics. This biosensor is composed by three parts: the first one is the transport and filtering layer for biological sample, the second one acts as a spacer holding the microheaters and the third one will be the electrical transducer. Nowadays Point-of-Care diagnostic devices have gained importance for rapid disease detection and personalised health monitoring.

The proposed objectives for the thesis are the following:

1. Produce the resistance layer;
2. Characterise the resistance and test the heater/temperature sensors for thermocycling;
3. Fabrication of the capacitive transducer;
4. Functionalisation with thiol-based SAM of the gold electrodes surface and grafting of the molecular sensing element (SS-DNA or antibody, or aptamer);
5. Characterise the capacitor before and after the functionalisation as well as after the hybridisation process with complementary DNA;
6. Analyze the changes made by functionalization and hybridization in the impedance of sensor;
7. Product of paper-based holder/filter microfluidics;



# 1. Introduction

Nowadays the response time in medical care is one of the biggest problems of medical services, being directly related with efficiency of treatment and mortality, it is one of the most pressing issues to be solved. In-Vitro Diagnostics (IVD) platforms are widely used for a variety of analysis of biological samples to provide crucial information for making right medical decisions.

Point-Of-Care Diagnostics (POCD) would benefit from IVD assays that can provide a quantitative analysis of given biomarkers: a) in a relatively short time (e.g. less than one hour), as needed to: i) prepare the sample, ii) process it with either manually-assisted or automatic operations, and iii) extract relevant quantitative information and raw data, that can be processed using a dedicated data analysis software on a generic computing platform, in order to provide an answer relevant to the specific infection disease, and b) with cost-effective solutions, this latter aspect being strongly influenced both by the cost of disposable cartridges where the sample is prepared and analyzed, and by the cost of reagents used to run the assay.

Various attempts have been done and are known in prior art to develop technologies that can be used as effective IVD platforms for POC diagnostics.

Present day technology for testing infection disease include antigen-related immunoassays, such as enzyme-linked immunosorbent assay (ELISA) and chemiluminescence immunoassays, and PCR (Polymerase Chain Reaction)-related molecular diagnostics. Antigen-based immunoassays require more amount of protein biomarker than molecular diagnostics. Molecular diagnostics is rapidly growing with the increasing adoption of this technology in place of antigen testing by immunoassays. Molecular diagnostics also have advantages such as high specificity which help to detect even a minimum amount of protein biomarkers in order to detect earlier infectious diseases.

This is why, responding to an unmet clinical need, POCD (Point-of-Care Diagnostics) has gained high interest by the scientific and industrial communities.

Point-of-Care testing (POCT) solutions are essential for the rapid detection of analytes near the patient, which facilitates disease diagnosis, monitoring and management [1]. Ideally Point-of-Care tests are made to be simple medical tests that can be performed at the patient bedside.

In this concept of device, the biosensor is the most critical component in the POCD and is directly responsible for the bioanalytical performance of an assay. Several prospective label-free biosensors, based on electrochemical, surface plasmon resonance (SPR) and white light reflectance spectroscopy (WLRS), have been developed and are used to improve POCD [1,2]. In many cases a sufficient level of cost-effectiveness and ease of operation is required to enable effective POCD, which in turns requires further development of the biosensor technology, not only to make the test possible but also to reduce its complexity. In fact, the envisaged miniaturisation of sensor chips and readout electronics pave the way toward completely new applications and markets in the field of bio-molecular diagnostics. Due to the ease of use of these highly integrated microsystems, Point-of-Care diagnostics, as in the doctor's office, comes into reach [3].

This can have even a bigger impact in the case of DNA (deoxyribonucleic acid) assays for molecular diagnostics, that require several amplification steps of targeted DNA sequences (amplicons) achieved through thermocycling via the well-known polymerase chain reaction (PCR) process.

Additionally, prior to amplification, sample preparation is required, involving a series of steps to extract the DNA from the sample, and to remove the different inhibitory compounds present in clinical samples of biological fluids. These steps often require the use of complex laboratory equipment and highly trained personnel. This combination of factors causes a late access to the test results. A reduction in

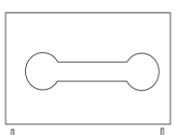

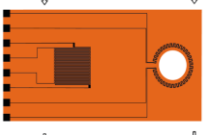


mortality has been associated with rapid turnaround times. This is where it comes the advantages of POCD applied to this type of assays making them rapid, simple, noninvasive and affordable [4–6].

The capacitance-based transduction is a very simple technique, resulting in simplification of the experimental procedure and the potential fabrication of portable systems, with lower costs reagents and smaller size, thus being suitable for Point-of-Care applications.

Assays using short single-stranded oligonucleotide probes immobilised on an electrode surface (transducer) can be used as highly sequence-specific recognition elements for the detection of DNA.

In this work is proposed a flexible POC device, for label free electric read out of Real Time quantitative Polymerase Chain Reaction (RT-qPCR), composed by three different layers as it is showed in Figure 1. The first layer will act as a medium of transport of the sample as the same time as it works as a filter and will use a paper substrate taking advantage of this material structure and using it as microfluidic device. The second layer - resistance layer - will take the fundamental principal of resistances and joule heating and thermoconducting detection to create microheaters and temperature sensors. The third layer the capacitive sensor uses micro fabrication technique to provide an interdigitated capacitor that will be functionalised to work as DNA sensor further on. The functionality of each layer and how they work will be explained in further detail, in the next chapters.

This type of approach is intended not only to have a better solution for bedside situations, but also to provide a device with a better sensitivity and low detection limits as result of the use of a capacitor as a transducer. This device was designed to be able to replicate the multiple laboratory procedure in just one device and even more, it can be used whether as a diagnostic system or a monitoring one, as the assays RT-qPCR allows.

1°		paper Whatman n°1	Microfluidics
2°		paper supor pore 200	
3°		Resistance layer (70nm Au and 10 nm Ti) Kapton	Thermocycler and thermolysis
4°		Su8 well	RT-qPCR sensor
5°		Capacitive sensor (70nm Au and 10 nm Ti) Kapton	

**Figure 1** Scheme of the sensor

## 1.1.RT-qPCR

With the increasing demand of clinical detection for DNA and RNA (Ribonucleic Acid) signatures in patients' diagnosis and monitoring at the Point-of-Care, the Quantitative Polymerase Chain Reaction (Q-PCR) becomes an extremely powerful and useful technique. This process enables to amplify fragments of DNA and determinate the amount of PCR product in real-time (also known as Real Time quantitative Polymerase Chain Reaction, or RT-qPCR). Therefore it has a vast application and it is widely used as a tool for investigating gene expression and gene analysis, identification of infectious diseases and clinical diagnostics [7].

RT-qPCR is also applied to detect nucleic acids from food and other microbiological uses, as water quality [8], vectors involved in gene therapy protocols, genetically modified organisms responsible to detect GMOs [9–11]. Another frequent uses of RT-qPCR assays include diagnosing [12] and monitoring diseases.

It is an important part of the assay to monitor the amount of PCR product over time and the effect that parameters such as melting temperature (TM) and primer concentration have on the reaction and that ultimately determine the detection threshold. The temperature at which the primer anneals is usually referred to as the TM. This is the temperature at which 50% of the oligonucleotide–target duplexes have formed [11]. The threshold cycle (Ct), represents the cycle when the sample fluorescence exceeds the background fluorescence. The Ct is used for quantifying the gene target copy number, however its value is entirely subjective, as the threshold can be altered at will [13].

The RT-qPCR uses the same principle as the regular PCR when it comes to the DNA amplification process. However, Real-Time qPCR methods allow for detection of PCR amplification during the early phases of the reaction. Measuring the kinetics of the reaction in the early phases of PCR provides a distinct advantage over traditional end-point detection-based PCR. Not only the overall time for analysis of the sample is shorter than it is for end-point detection, but, it also offers the unique advantage of focusing the detection phase during the exponential phase, which is the optimal point for analyzing the data, when all reagents are fresh and active and amplicons double effectively at every thermal cycle and no degradation mechanism occur, which in turn results in more accurate DNA or RNA quantification and does not require laborious post-PCR methods.

It is the detection process that discriminates real time PCR from conventional PCR assays [11]. The main difference between them is the fact that PCR is just a DNA amplification tool. This means that its purpose is just to take a small piece of DNA and amplify it, in order to allow other methods of DNA detection to read it. Furthermore, RT-qPCR is an amplifying process which permits to track this amplification in real time, mostly due to DNA probes mixed in the process with a fluorescent label. Another function is to supply other types of information as if the sought gene is present in the sample or not, with no need for other methods, it also gives a quantification of gene expression. The more common fluorescent probes used in this method are SYBR Green and TaqMan [14].

However, this work will follow a different approach, which does not require use of fluorescent probes reagents. The aim is to enable electronic read out of the amplicons concentration during thermocycling, hence called “label-free” detection, which means no need for optical read out based on fluorescent molecules. This approach would permit a drastic reduction in the use of large readout machinery and its associated maintenance, besides a reduction of the cost of reagents and the time-consuming data processing involved in the interpretation of fluorescence data involved in standard RT-qPCR. A small amount of deoxyribonucleic acid (DNA) fragments are processed into a plurality of sample products during the thermal cycles as shown in Figure 2 c) and b) [7].

Using a polymerase enzyme that recognizes the DNA via primers, regardless of the method used to synthesize cDNA, the PCR step requires a specific target primer. These are usually designed in isolation, using single templates of very limited genetic complexity [13, 15].



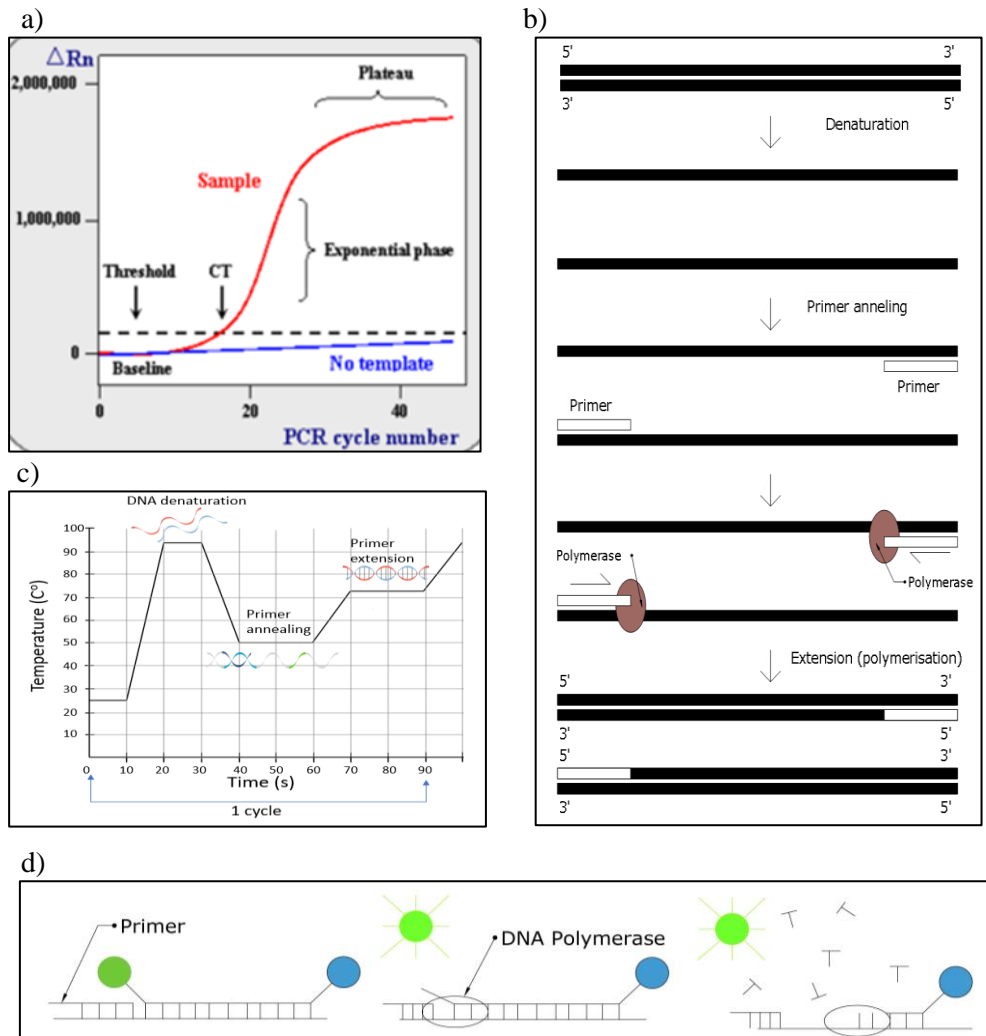


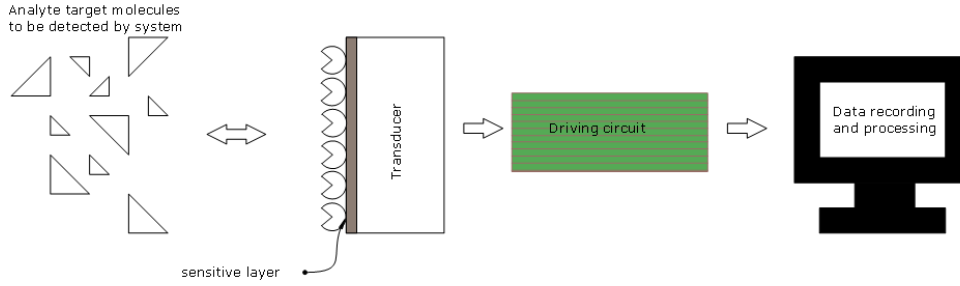
Figure 2 a) Shows theoretically the type of response that we will obtain with an optical RT-PCR. Adapted from [16]; b) One cycle of PCR; c) Thermocycler graphic; d) Schematic of an example of fluorescent assay TaqMan probe qPCR

In a standard RT-qPCR assay the solution would contain a labelled DNA probe with a reporter fluorescent dye [FAM (6-carboxyfluorescein)] at the 5' end and a quencher fluorescent dye [TAMRA (6-carboxy-tetramethylrhodamine)] at the 3' end, this probe would bind to the target gene after the primer. When the probe is intact, the photo emission dye usually reported is quenched due to the physical proximity of the reporter and quencher fluorescent dyes. However, during the extension phase of the PCR cycle, the DNA polymerase nucleolytic activity cleaves the hybridisation probe and releases the reporter dye from the probe. The resulting relative increase in reporter fluorescent dye emission is monitored in real time during PCR amplification using a sequence detector Figure 2 d) [15].

The Real-Time PCR requires a thermocycler in combination with an optical system to capture fluorescence and a computer with software capable of capturing the data and performing the final analysis of the reaction giving a graphic similar to the one shown in Figure 2 a) [11,14,15].

## 1.2.Capacitive Sensor

A sensor is a device that detects a signal and converts it into a measurable quantity. A biosensor consists in a biological recognition element in close proximity to a transducer, which will convert the binding event into an electrical signal [17].



**Figure 3 Schematic of sensor based on [18].**

Biosensors can be defined as chemical sensors where the recognition system detect a biochemical mechanism. The biosensors can be repeatedly calibrated and are suitable for monitoring both the increase and decrease of the bio-analyte concentrations [19]. The Figure 3 represents the schematic of sensor and how it works.

Lately the capacitive transducers have become promising in the field of immunosensors and in the detection of bioavailable heavy metal ions, giving both high selectivity and low detection limits. It was therefore considered as a suitable transducer for DNA detection, which is in the scope of this work [20].

The use of interdigitated electrodes (IDEs) for the development of sensors has been receiving growing interest during the last two decades. The fabrication of the IDEs by means of lithography allows the development of sensitive, low cost and miniaturised chemical sensors and biosensors.

In the field of interdigital capacitive (IDC) sensors, the principle of detection is based on the change of the dielectric constant in the medium of the interdigitated capacitor. The change in the dielectric constant of the medium is an effect of the electrical double layer theory, which can be described as a build-up of two conducting phases. One consists in a metal surface and the other in an electrolyte solution as it will be explained in further detail later. The capacitance of a sensor is a function of the dielectric permittivity, the materials of the sensor and the geometry as is shown by expressions (1) and (2). The modification of the interface between the metal surface and the solution by immobilising a recognition element will lead to a change in capacitance value, which will be dependent on the nature and coverage of the recognition element. Further change is expected when the analyte binds to the recognition element [20]. In the present work the principle of a capacitor device consists in changing the dielectric permittivity of flat capacitor structure under the influence of external factors [2].

A simplest view of the sensor type capacitance is to view them as two close-spaced parallel plates. Therefore, the capacitance between the two electrodes is given by:

$$C = \epsilon_r \epsilon_0 \frac{A}{d} \quad (1)$$

where  $A$  – the area of facing plates,  $d$  – distance between the plates,  $\epsilon_0$  – permittivity in vacuum,  $\epsilon_r$  – is the relative permittivity of the dielectric layer [21,22].

However, capacitive devices working as biosensors like the case presented in this work whose operation is based on the changes of the permittivity of the biological material are subdivided into two categories: interdigitated electrodes (IDEs) and electrode–solution interfaces. In the simplified case where the electrodes are thin compared to the surface area (80 nm of thickness and 0.25 mm<sup>2</sup>) and where first fingers may be neglected and considering an infinite layer, the capacitance of an IDE sensor is given by:

$$C \cong \left(\frac{n-1}{2}\right) C_i L \text{ where } C_i = \epsilon_r \epsilon_0 \frac{K(k_{1\infty})}{K(k'_{1\infty})} \quad (2)$$

$$k_{1\infty} = \operatorname{sen}\left(\frac{\pi}{2}\eta\right) \text{ and } k'_{1\infty} = \sqrt{1-k}$$

$$\eta = \frac{W}{W + G}$$

where  $n$  is the number of the fingers,  $K(k)$  is the complete elliptic integral of first kind with modulus  $k_{1\infty}$ ,  $k'_{1\infty}$  the complementary modulus,  $L$  is the length,  $\eta$  is an adimensional parameter,  $W$  the size of the finger and  $G$  is the distance between the electrodes as it is shown in Figure 5 b) [23]. This equation gives us the geometrical capacitance which is the sum of the capacitance of two other capacitances, one taking in account the medium on top of the electrode and the other one taking in account the subtract.

### 1.2.1. Impedance

The project enlightens the changes in the impedance of the device instead of capacitance measurement, being the impedance the ratio between voltage and current [24].

The electrochemical impedance spectrum is obtained by measuring the electrical current response in dependence of the frequency of the applied voltage. In any electrical circuit comprising capacitive and resistive elements exposed to an alternating voltage there will be a phase difference between the electrical current and the applied voltage in dependence of the frequency ( $f$ ). This is conveniently represented by the complex impedance  $Z$ :

$$Z(f) = Z' + jZ'' \quad (3)$$

where  $j$  represents the imaginary unit  $j = \sqrt{-1}$ . The data are typically displayed in a plot of  $-Z''$  against  $Z'$ , (Nyquist plot) [25]. While this does not show the frequency dependence of the impedance directly, the data points obtained at the highest frequencies, are in the most left part of the plot and those obtained at the lowest frequencies are at the right.

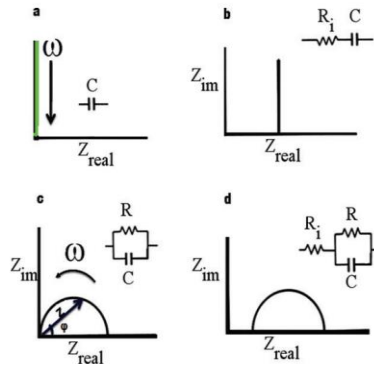


Figure 4 Behaviour of each component in the Nyquist plot. Adapted from [26]

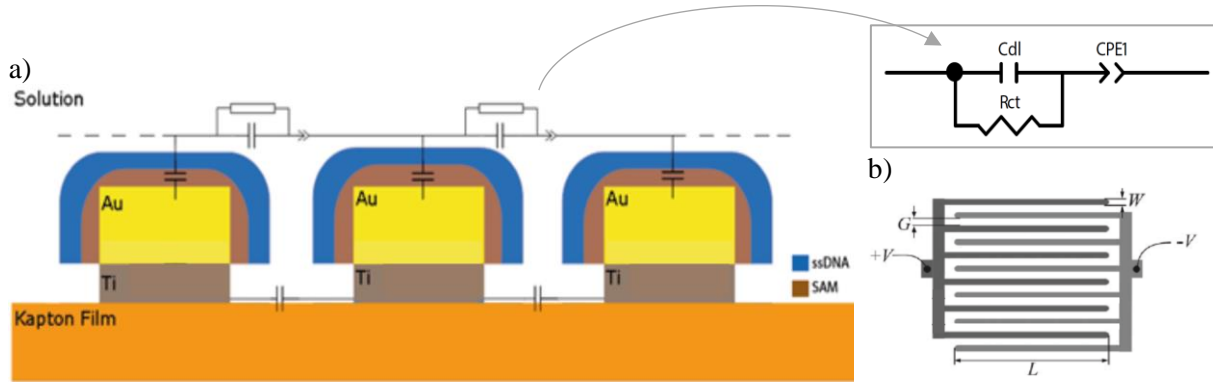
It is worth of notice that the plot  $Z'$ ,  $Z''$  showed in the Figure 4 is the typical behaviour of each electrical component.

The curve obtained with the Nyquist plot can be fitted to a model of an electrical equivalent circuit (Figure 5), allowing interpretation of the surface properties of the device, in terms of electrical circuit elements. One drawback of this approach, is that interpretation of the data requires an iterative curve-fitting algorithm and user input, which is not readily accommodated in a mobile device [26,27].

#### 1.2.1.1. Electronic model

According to the literature, the electronic model represented in Figure 5 is a good fit to represent what happens in the devices in study. A single capacitor is certainly too simple to mimic the impedance

found with real biomaterials at all frequencies. A much better fit can often be obtained by using a non-ideal component which is frequency dependent.



**Figure 5 a) Cross section of EIS with electric equivalent circuit adapted from [29] b) Schematic of the top view and features adapted from [23]**

From an electrical point of view, the electrode solution interfaces are characterised by capacitive and resistive parameters, both sensitive to the state of the electrode surface followed by a constant phase element CPE. In this circuit, the addition of CPE on the circuit is necessary, which can be ascribed to block the diffusion process. Accordingly, the charge separation occurs and the interface acts as a non-ideal capacitor (CPE) [30].

The additional capacitive impedance  $Z$  is due to the adsorption and desorption of species at the electrode surface. These species do not exchange electrons with the electrode surface but changes the surface charge density and cause a pure AC (Alternating current) current path. Under ideal conditions the concentration at the electrode surface is  $+45^\circ$  and the voltage  $-45^\circ$  out of phase with the applied current, independently of the applied frequency. The impedance of the constant phase element is given by:

$$Z(\omega) = \frac{1}{Q} (j\omega)^{-n} \quad (4)$$

where  $\omega$  is the frequency,  $0 < n < 1$  and  $Q$  is a constant with dimension  $F \cdot s \cdot n^{-1}$ . The case of  $n = 1$  it recovers as a perfect capacitor while the case  $n = 0$  describes a pure resistor [31].

If this hosts a layer of probes that can form chemical bonds with complementary DNA targets in solution, such a reaction (selective hybridisation) affects the value of interface electrical parameters and this variation can be detected. Is expected, in particular, a decrease in the interface capacitance of gold electrodes due to DNA hybridisation [32].

### 1.2.1.2. Electrical double layer

When a membrane has fixed charges in equilibrium with an electrolyte solution, an electric potential difference is generally established between the membrane and the solution [33]. In this model is envisaged that no electron transfer reactions occur between the electrode and the solution which is composed only of electrolyte. The interactions between the ions in solution and the electrode surface, were assumed to be electrostatic in nature and resulted from the fact that the electrode holds a charge density ( $qm$ ) which arises from either, in excess or deficiency, of electrons at the electrode surface. In order to maintain the interface neutral, the charge held on the electrode is balanced by the redistribution of ions close to the electrode surface.

The attracted ions are supposed to approach the electrode surface and form a layer which will balance the electrode charge. The overall result is two layers of charges (the double layer) and a potential drop in the solution. The outcome is analogous to an electrical capacitor which has two plates of charge separated by some distance, with the potential drop occurring in a linear manner between the two plates.

The electrical double layer plays an essential role in various interfacial electrical phenomena observed in a suspension of colloidal particles.

However, the physical models for this kind of system are still to be perfected and unified. For this reason, it will be considered the Stern model which takes into account diffusion/mixing in solution, the possibility of absorption on the surface and the interaction between solvent dipole moments and the electrode [34]. Now the ions are assumed to be able to move in solution and so the electrostatic interactions are in competition. The result of this model is still a region close to the electrode surface (10 nm) containing an excess of one type of ion with the potential drop occurring over the so-called diffuse layer.

### **1.3. Microheaters and heat sensors**

Microheaters are small high-power heaters with precise control that provide an accurate high temperature control. Generally speaking, the heating method for microheaters involves conversion of electrical work to high density heat. With the use of high temperatures, the microheaters need to be supported or enclosed with very high thermal-resistant materials often made from small grain and high purity. The main advantages of incorporating such kinds of devices are flexibility, rapid prototyping and great compatibility with existing flexible chips [35].

Microheaters and temperature sensors usually play important roles in biological processing and chemical reactions. Hence, microheaters have been widely applied to heat chemical in solution, providing rapid thermal cycling process in polymerase chain reaction PCR microfluidic devices [34,35].

### **1.4. Microfluidics**

The need of development in Point-of-Care diagnostic tests (POC) and home-care medicine, where user-friendly, portable and low-cost systems can be used at the doctor's office or directly by the patients themselves to monitor their health or detect bacteria and viruses from a blood prick led to Microfluidics [37]. Contrary to the conventional microfluidic solutions, the requirement for portability and low cost is associated to the development of passive or nearly passive solutions. Spontaneous capillary flow (SCF) is a capillary flow occurring spontaneously under the action of a negative Laplace pressure at its front end while the rear end is at zero (relative) pressure. Sometimes SCF can be a drawback in microsystems, other times it can be purposely used for fluid actuation [37].

It became obvious, the need for capillarity as a solution, for moving liquids under these conditions. In a capillary solution, the energy required for the motion of the fluids is the surface energy of the walls, which is built at the moment of fabrication or by appropriate functionalisation of the walls [38].

The term "Microfluidics" refers to a technology which manipulates small volumes of fluids, with the potential to miniaturise complex laboratory procedures into a small microchip. The great advantages of using smaller volumes of samples and costly reagents, compared to macroscale devices, are the time consumption (operating time is much shorter), the simplicity of the analyses process, a higher sensitivity and the possibility of mass production [37–39]. Microfluidics is used as an adequate transport, concentrating and filtering the biochemical targets or the biologic objects.

The cellulose paper is naturally hydrophilic and allows the penetration of aqueous liquids within the matrix fibers, the process of spreading is explained with further detail in annex 1. However, the design of a path way for liquids is accomplished by coating the paper fibers with hydrophobic materials and this way is obtained channels that guide the fluid inside the paper [40,41].

For a DNA probe assays, genomic molecules, infective bacteria, or virus particles are required in average a concentration range from 100 to 10<sup>7</sup> copies per milliliter. The relation between the sample volume  $V$  and the analyte concentration  $A_i$  can be calculated by the equation 7 present in annex 7 [39].

# 2

## 2. Methodology

In this chapter it will be explored the processes behind the fabrication, the materials and the characterisation of the devices proposed in this study, as well as how the results presented in the next chapter were obtained.

### 2.1.Overall view of layers of the device and the setup

With following images, we pretend to show progress and the overall process of the device

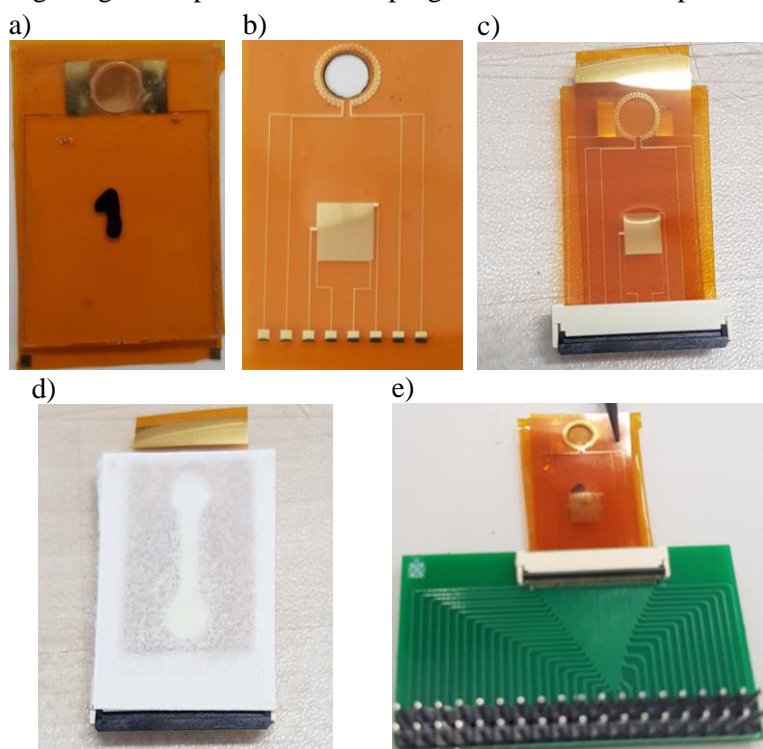


Figure 6 The different layers of the device

The device presented in figure 6 is composed by three different layers: a) the capacitive biosensor (a capacitor capable of detecting hybridization events by DNA probes); b) the resistance and thermosensors which replaces the thermocycle process; c) the first two layers are on top of each other and designed to link a ZIF connector; d) a transport layer and filter made by paper; e) the study of the two kapton layers, linked to the ZIF connector which was mounted already on a PCB, that could be installed with a controller that allowed the recording, managing and processing of the obtained data.

### 2.2. Microfluidic process

In order to obtain a transporter and filtering layer for the biological sample it was used paper subtract. This paper was then printed with the EMD6415 ink (bought from Sunchemicals Company) that was referred in the lecturer as able to produce hydrophobic walls in the paper [43]. Therefore, to build the hydrophobic walls, it was used an inkjet printer Dimatix 5200 from Fujifilm. The process would take 20

layers of ink with a heated stage and direct UV light during the printing process, to avoid undesired spreading of the ink through the paper, was used a flashlight of 100 LEDs (Figure 7 b)). It was also studied different types of papers with different pores size to see which one would fit best the desired purpose. Results are displayed in the next section, linked to the results for hydrophobicity of the ink on each paper type.

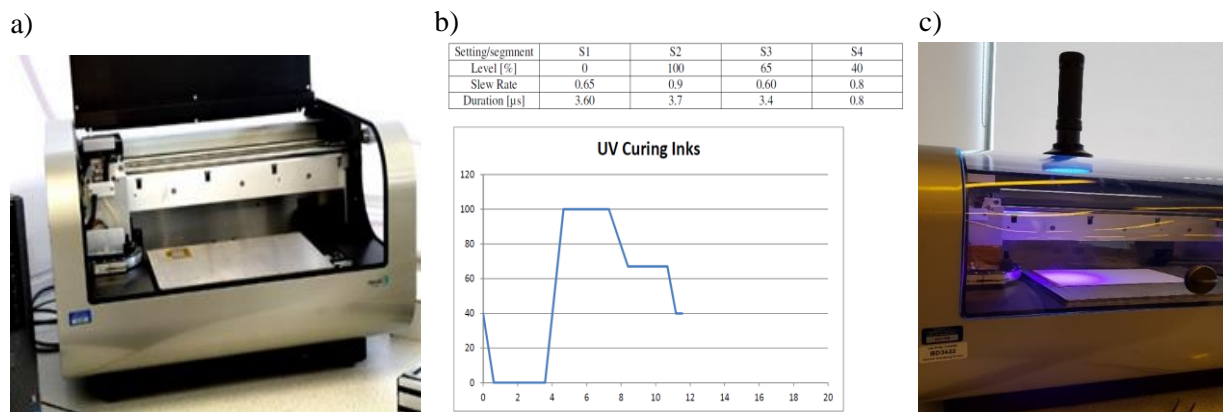


Figure 7 a) Inkjet Dimatix 5200; b) Waveform for EMD6415; c) Setup used to fabricate microfluidics

The design was made using *Adobe Illustrator* software and it was based on previous biosensors with paper base microfluidics.

### 2.3. Contact angle technique

Nowadays the most common method to determine the hydrophobicity of a material is the contact angle present in Figure 8. The term contact angle refers to the angle made by the interference of systems formed by materials with different physics states. The most common system is the gas-solid- liquid, where it is assumed that the interaction surface of the solid is flat. The contact angle is defined as the boundary condition on the solid surface that incorporates the physical properties that will govern the shape of the liquid-vapor interface. In an ideal system, a homogeneous solid surface, the formation of balance of forces in the contact line can provides a contact angle value based on the energy density of the tree interfaces of system [44]. This balance is generated by Young's equation, which can be derived by minimizing the mechanical energy of the system for the different areas of continuous, liquid and gaseous contact:

$$\cos(\theta_c) = \frac{\gamma_{SG} - \gamma_{SL}}{\gamma_{LG}} \quad (5)$$

where  $\theta_c$  represents the contact angle,  $\gamma_{SG}$ ,  $\gamma_{SL}$  and  $\gamma_{LG}$  represent the surface tension of the solid-gas, solid-liquid and liquid-gas interfaces, respectively. Through Young's equation it is possible to verify that there is a close relationship between the contact angle and the surface tension. Thus, in order to measure the contact angle, at least one of the three surface tensions presents in the equation 5 must be known [45].

If the contact angle is greater than  $90^\circ$  the substrate is considered as hydrophobic, as there is no good adhesion between the surfaces of the materials in contact. If the angle found is less than  $90^\circ$  the substrate is hydrophilic, as adhesion between the materials is favored.

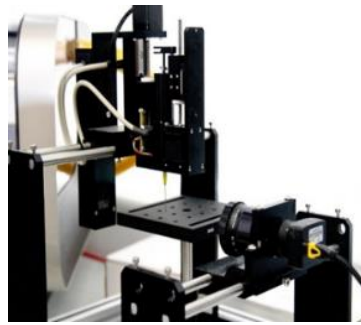


Figure 8 FTA 1000 Analyser System

## 2.4.Fabrication

All the fabrication process was performed in a clean room environment. To fabricate the devices, it was used a Kapton film substrate, due to the fact that polyimide-FEP fluoropolymer composite film with unique and excellent electrical balance, thermal durability and chemical resistance properties [46]. This polyimide film was then submitted to several cleaning processes. First, it was processed with the cleaning process which relay in bath of acetone for 5 minutes followed by a bath in IPA solution for another 5 minutes and after this, it was cleaned furthermore with an oxygen plasm treatment. Additionally, the films where put through a heating treatment before going into the lithographic process. This treatment had the objective to evaporate any solvent left or any water that could be remaining in the film, as a way to avoid disruption in the metallic films as first appeared in the fabricated devices, as it is shown in the annex 5. This treatment also prevents the bending during the baking process in the photolithographic steps.

In order to fabricate the devices, it was used two types of Kapton film. However, as shown in the annex 4, in the first type kapton (25  $\mu\text{m}$  of thickness) the surface to rough, with a lot of deep scratches which would result in disruption of the metal lines. Therefore, it was decided to use the thicker version which seems to have a smoother surface (with a thickness of 50  $\mu\text{m}$ ).

With the help of *Autocad* and *Cleawind* software it was made the design of both the capacitors and resistances. To ensure that these designs would work, it was firstly tested using a laser writer tool LW405C from a Microtech Srl company represented in Figure 9 a). This tool allowed to test the features sizes and the design of the devices, by using a laser bean to write as a lithography method. This method does not require a photolithographic mask, since it works as printer, scanning the sample and exposing the desired parts according to the draws previously made in the *Cleawind* software.

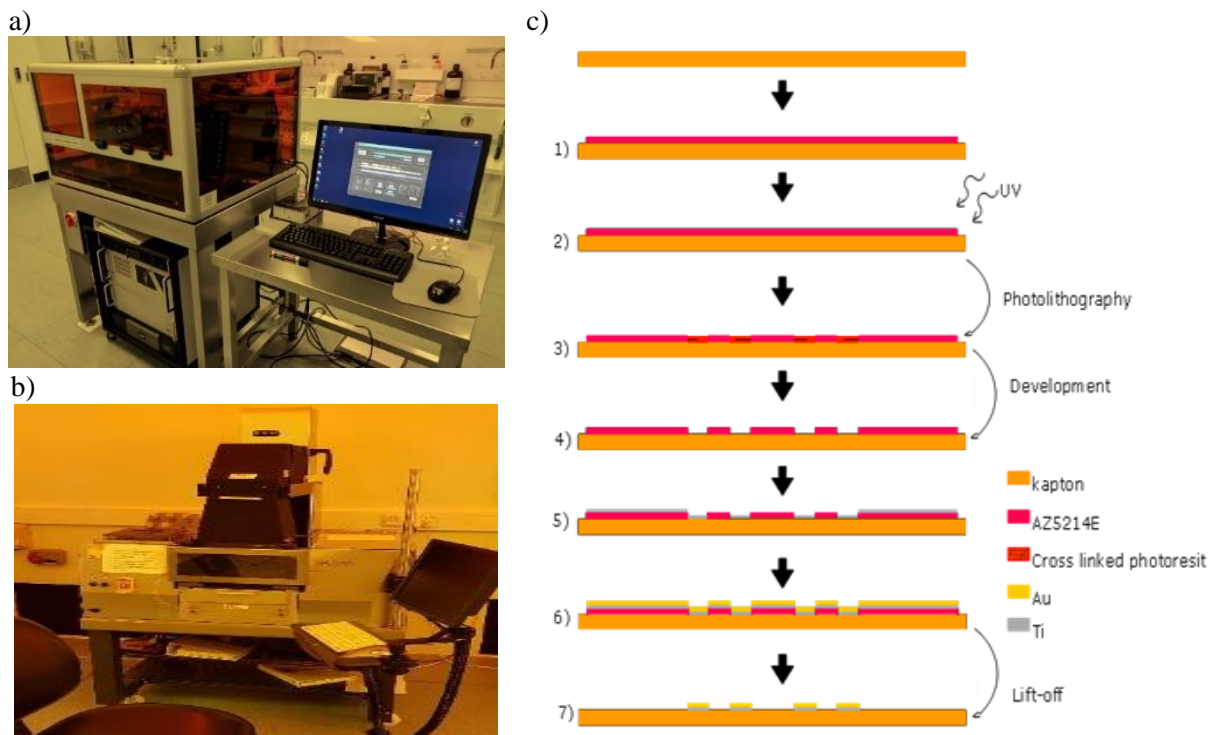
Its already known that, the fabrication and rentability of large area devices in flexible substrates is a challenging process. Moreover, the smoothness of the surface of this kind of substrates sometimes presents a challenge to the fabrication steps, as this are mostly optimised to silicon wafers. They were designed with pads to match a ZIF connector (zero insertion force) which have a pitch size of 0.5mm, but to increase the current put through, the pads were made to cover two pitches. After this process it was commissioned a mask to JD company to increase the productivity of process. Then it was used Mask Aligner - MA/BA6 Figure 9 b) with the designed mask.

The capacitor was designed with the same wide line of the resistances 50  $\mu\text{m}$ , to have 25 fingers each electrode and a  $d$  value (space between fingers) of 50  $\mu\text{m}$ . Also, it was made some tracks to the ZIF connector pads in order to allow the correct position under the well were all the reagents will be mixed.

### 2.4.1. Photolithography with AZ photoresist

After the cleaning steps, the Kapton film samples were spin coated with AZ5214E photoresist, using a 4000 rpm during 30s with an acceleration of 1000 rpm for a thickness of 1.4  $\mu\text{m}$ , followed by a post bake of 100°C process for 1min.





**Figure 9** a) Laser writer; b) Mask Aligner - MA/BA; c) Photolithographic process

The samples were then exposed in Mask Aligner - MA/BA6 from Suss Company using hard contact mode for 8 sec, with a 0.3 mbar WEC pressure. The UV light was turned on, at least 20min before being used to ensure maximum UV power. After 5 min, the sample was post baked at 125°C for 45 sec. However, between the post bake and the flood exposure the sample had to wait for 5min at least.

The flood exposure (soft contact, no mask) took 29.9 sec. Development took 20 sec in AZ351B mix with deionised (DI) water in a ratio 1:4 and finally were rinsed in DI water.

### 2.4.2. Metallization process

The metals deposition was obtained with e-beam evaporator PVD200 from Kurt J. Lesker Company. First it was deposited an adhesion layer of 10 nm Ti with a rate of 1Å/s followed by a second deposition of gold with 70 nm Au with the same rate.

Lift-off process was accomplished by putting the sample in a bath of acetone to remove the resist that was not cross linked and that remained after the development process. This process also removes the metals deposited on top of this resist, leaving only the metals in the paths that were opened in the development process. To avoid unwanted removal of materials, the samples were left over-night in the acetone bath allowing a slow lift-off process. The process of metallisation and the photolithography are represented in Figure 9 c). After the metallisation process the layers were characterised as shown in 2.2 chapter.

### 2.4.3. SU8 well

In the Kapton substrate it was built a well to contain the solutions, on top of the capacitor necessary for the RT-qPCR assay. This well was obtained using a SU8 material, due to its properties and accessibility and it was designed to be as thick as possible using SU8 2100, which has a maximum thickness of 300 µm.

In spite of the possibility to use a SU8 to produce a thicker film, this was limited by the photolithographic process and the use of lens 6 (the only lens capable of using the necessary 375nm wave length to cure a resist this thick) in the laser writer Figure 9 a)).

However, this means that the sample would have to pass through lens 5 which is the biggest magnification and physical structure. To ensure that lens would not crash with the sample it was necessary to consider this limit. For this reason, we were limited to 300  $\mu\text{m}$  of thickness.

The first step of the well fabrication was a cleaning process with acetone ultrasonic bath in for 5 min and rinse with IPA. The SU8-2100 was first spin coated at 500 rpm for 10s, for a more homogeneous spreading, followed by 1000rpm for 30s giving the desired 300  $\mu\text{m}$ . The samples were then pre-baked at 65°C for 5 min and 95°C during 20 min. The process was followed by the exposition step with the laser writer tool, using lens 6 (375nm) with a setting of exposition, a gain of 20 and D-step of 4.

After the exposition the samples were post baked at 65°C for 5 min and then subjected to 95°C for 15 min. However, a second exposition for thick film is recommended, hence a second post bake is required with a temperature of 150°C for 5 min.

Before the development, the samples were left to wait 2-3h. To develop the devices were put in a solution of PGMEA for 10 min and then rinse with IPA and Acetone.

The goal of producing a thicker film of SU8 was to contain the volumes of the solutions needed to realise the RT-qPCR assay. As it can be seen in section 2.5. (RT-qPCR process) this assay requires a volume of 20  $\mu\text{L}$  with the design of a circular well with a diameter of 5mm given its geometry, the ideal thickness with this volume would be around 500  $\mu\text{m}$ . It was possible to do the assay with the required volume using a well with just 300  $\mu\text{m}$  thanks to the cohesion forces of the.

## 2.5.Characterisation

After the fabrication step, the two layers of the device (resistance and capacitor), were characterised using a Cascade probe station represented in Figure 10 connected to a Semiconductor Device Analyser B1500A from Agilent Technologies Company.



Figure 10 Cascade probe station.

### 2.5.1. Impedance spectroscopy

The impedance spectroscopy was obtained using the Cascade probe station (Figure 10) and with the Precision Impedance Analyser, 4294A from Agilent Technologies. The measurements were made with an oscillation voltage the 10mV and using a 4 probes method.

## 2.6.Functionalisation of the capacitor

The process to functionalise the capacitor was made in different steps and it was based on the methods of Eleonora Macchia [47] and Andreas Kukol [28]. This two methods were used in combination with the propose of having a highly dense layer of small thiols that would make a hydrogen bond network as reported in Eleonora Macchia [47] method that would improve the sensibility. As well as longer thiol groups in the middle of the network of smaller ones that was reposted in the Andreas Kukol [28] also increase the sensitivity of the sensor.

### 2.6.1. Cleaning step

The surface of the golden capacitor was submitted to a cleaning process. Firstly, the sample was cleaned by ultrasonic baths of isopropanol for 10 minutes, then oxygen plasma and finally UV/ozone cleaned for 10 minutes [18,22].

### 2.6.2. Preparation and Functionalisation

The thiol group provides a covalent bond with gold atoms in the surface of the electrode and the small alkali chain acts (depending on its length) to form a compact layer. Molecules can be deposited by microspotting, ink-jet printing [34], or deposited on the surface by immersion (dipping) in a micromolar concentration solution [22]. In this study it was used the dipping approach in order to functionalise the electrodes.

The golden dielectrics were dried briefly in a stream of nitrogen and put after in a 10 mM solution consisting in a 10:1 molar ratio of 3-MPA to 16-Mercaptohexadecanoic acid that was prepared in ethanol solution. The devices immersed in the 3-MPA and 16-Mercaptohexadecanoic acid solution were kept in the dark, under constant Ar flux for 18 h at 22 °C. To ensure these conditions this process was performed in a glove box chamber covered in black foil. The carboxylic groups were activated afterwards in a 200 mM EDC and 50 mM N-Hydroxysulfosuccinimide sodium salt aqueous solution for 2 h at 25 °C. The Primers capturing in the self-assembling monolayer (SAM) was generated, subsequently, through conjugation between the amine groups of the DNA single string and the activated carboxylic groups on the gate surface. This was obtained by immersing the electrodes in an DNA primers phosphate buffer saline (PBS) solution for 2 h at 25 °C.

The solution was composed by 1  $\mu$ L (300mM at 20  $\mu$ L) of DNA primers and 10mM (KCl 2.7mM and 137mM NaCl) of PBS with pH of 7.4 and an ionic-strength of 162 mM. Afterwards, to saturate the unreacted sulpho-NHS groups, the DNA primers SAM were further treated with ethanolamine 1M in PBS 10mM for 1 h at 25 °C. This latter step act as “chemical-blocking”. Finally, the biofunctionalised electrode was immersed in a 1.5  $\mu$ M (0.1 mg ml<sup>-1</sup>) BSA solution in PBS 10mM for 1 h at 25 °C. This step of BSA physisorption is addressed as the biological blocking of the electrodes surface.

After each step of the functionalisation protocol, the electrode was rinsed thoroughly in water, to remove possible residues.

### 2.6.3. Rinsing process

The electrode was rinsed for 2 min in buffer (100 mM phosphate buffer [pH 7.2], 100 mM NaCl and 5 mM MgCl<sub>2</sub>) before measurement of the impedance spectrum.

## 2.7. Hybridisation Studies

The specificity of a DNA probe depends on its length, composition and binding conditions such as: pH, salt content, solvent and temperature. The specificity of the binding will increase with increasing temperature and decreasing salt content. Oligonucleotide probes are chemically synthesized, with a length of up to 40 bases. To selectively detect a unique human DNA sequence, it has been reported that the DNA probe must have at least 16 bases.

When a specific DNA sample hybridize to oligonucleotides immobilised on the surface of an electrode, water and electrolyte molecules will be displaced by the DNA sample thereby giving a change in capacitance. The detection principle is shown in Figure 11. Single stranded 178-base oligonucleotide self-assembled on the electrode surface gave rise to a decrease in capacitance when functionalised [20,47].

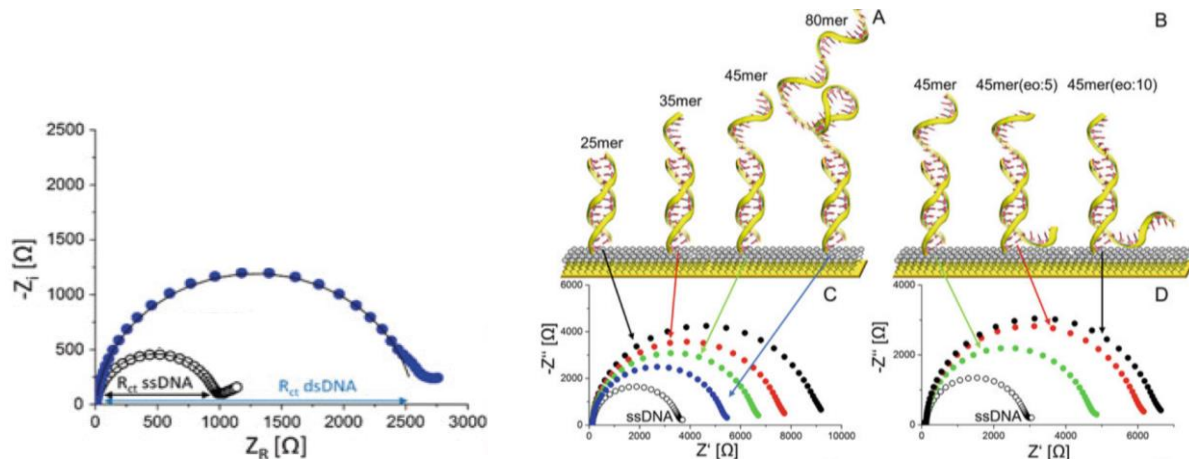


Figure 11 The relation between the hybridisation and the impedance adapted from [2].

In this study it was used the YWHAZ gene primer (tyrosine 3-monooxygenase/tryptophan 5-monooxygenase activation protein, zeta polypeptide) with the sequence (5'→3') ATGCAACCAACACATCCTATC GCATTATTAGCGTGCTGTCTT and a  $T_M$  60°C for 178 bp (base pair) [48,49]. The protein encoded by this gene on chromosome 8 is part of a member of the 14-3-3 protein family and a central hub protein for many signal transduction pathways [50,51]. This protein is a major regulator of apoptotic pathways critical to cell survival and plays a key role in a number of cancers and neurodegenerative diseases [52,53].

## 2.8. RT-qPCR process

The RT-qPCR assay was obtained using a master mix from Thermofisher (Platinum Superfi PCR Master Mix). This solution would contain the polymerase enzyme and dNTP's. The primers necessary to this process were obtained through Primer Design Company. In this study it was used the human reference *ywhaz* gene primers kit that would contain the primers for the gene as well as the double dye probe Taqman. Even though this double fluorescent probe is not useful for this study and when put in solution with the thiol groups on the gold surface is not supposed to bind. For this reason, it is expected why is expected to be washed away in rinse process. From this company was also obtained a positive control group, in order to study the hybridisation process.

The procedure for this experiment, was to pulse-spin each tube in a centrifuge before opening at max rpm for 30 seconds. This will ensure that lyophilised primer and probe mix will be in the base of the tube and are not spilt upon opening the tube.

The lyophilized primer was resuspended and probe by mix with 990  $\mu$ L of DNase free water (there is a 10% over pipette in each kit). To ensure complete resuspension, vortex each tube thoroughly, allowing it stand for 5 minutes and vortex again before use.

Then it was pipetted 1  $\mu$ L of this solution into the SU8 well and left, carried on with the functionalisation protocol that was already explained.

For the human positive control template sample the process of and pulse-spinning each tube in a centrifuge at max rpm for 30 seconds was repeated. Afterwards, resuspended the positive control template in 500  $\mu$ L on the preparation buffer template. To ensure complete resuspension, each tube was vortex.

This component contains a high copy number template and has a very significant risk of contamination. It must be opened and handled in a separate laboratory environment, away from the other components.

**Table I Contents necessary for a qPCR as for the respective volumes**

Solution	Volume
Resuspended primer/probe mix (anchored to the gold surface by the thiol groups)	1 $\mu$ L*
Platinum Superfi PCR Master Mix	10 $\mu$ L
RNAse/DNAse free water	5 $\mu$ L
Final volume	16 $\mu$ L

\*working concentration of primers = 300nM in a 20 $\mu$ L reaction

Then it was pipetted 15 $\mu$ l (1 $\mu$ L of the primers was already used) the of this mix into each plus 5 $\mu$ l of the positive control template. Making a final volume in each well of 20 $\mu$ L.

After this solution was dropped on well made with SU8 to react with the primers anchored to the surface, the sample was put thought the thermocycling show in Figure 2 c).

### 2.8.1. Thermocycling

A PCR process goes through three major steps during the thermocycle process as it is demonstrated in Figure 2 c) and Figure 2 b) [7,11]:

1. Denaturation - the double-stranded DNA (dsDNA) is separated into two single strands at about 95°C during denaturation for 10 sec (the first denaturation needs 30 sec);
2. Annealing – the oligonucleotide primers bind specifically to their complementary site of the single-stranded DNA at about 60°C for 20 sec;
3. Extension - DNA strands are extended by a thermostable DNA polymerase at about 20 sec at 72°C during the extension.

After each cycling process the device was taken to the probe station to get impedance values [5].

### 2.9. X-ray photoelectron spectrometer

The X-ray photoelectron spectrometer was an Axis Supra from Kratos Analytical, running a monochromatic AlK $\alpha$  source at 300 W. Surveys and images were collected at a pass energy of 160 eV and detail spectra at 20 eV. Since the DNA was only located on the 50  $\mu$ m contact lines, the image mode was used to center the analysis location on one of the contact lines. Then the spectra were collected with an aperture of 55  $\mu$ m. The total measurement time was around 20h.

# 3

## 3. Results and Discussion

In this chapter, the results concerning the resistance characterisation, impedance spectroscopy of capacitors, contact angle values, films characterisation and electric characterisation of heat capacitance and calculation of the device sensibility will be presented and discussed.

### 3.1. Microfluidics

By choosing the commercial ink EMD6415 the process of printing was only possible using a cartridge with a 10 pL nozzle and by introducing the wave form in Figure 7 b) into the Dimatix. It was also needed to configure the printer nozzles to be at 60 °C and with a voltage applied of 18 V. With all this condition it was obtained the jetting observed in the images in Figure 12.

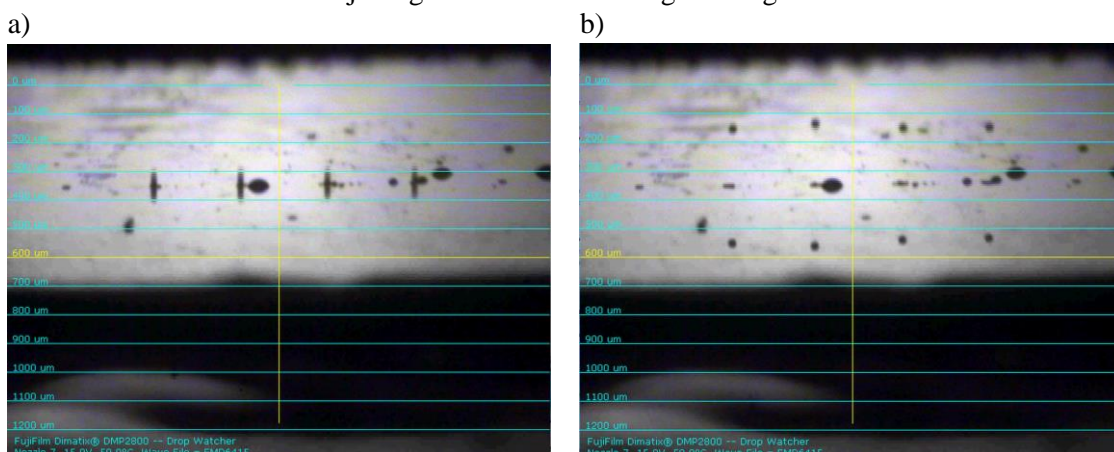


Figure 12 Dimatix jetting and droplet formation a) Drop coming out of the nozzle; b) Jetting of the drops

The Figure 12 shows what is to be considered a good jetting: Showing single drops with no satellites and straight jetting. To make sure of the hydrophobicity walls created inside the paper, it was performed a contact angle study.

The surface energy of cellulose fibers and paper is a parameter that affects their performance in terms of liquid penetration and adhesion to other polymeric materials. The hydrophobic properties of the studied substrates were determined using FTA 1000 Analyser System equipment, shown in Figure 8.

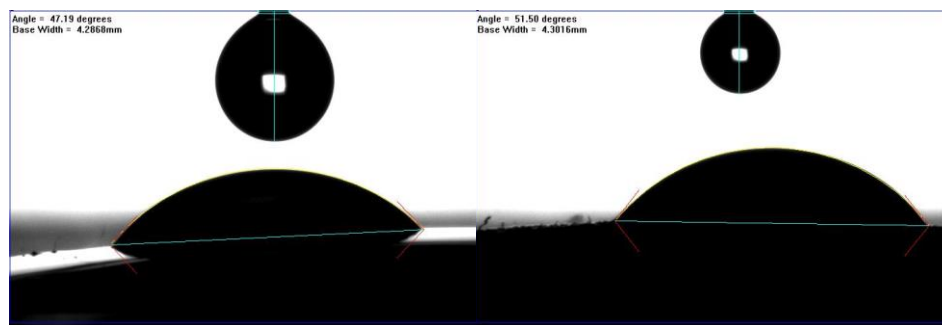
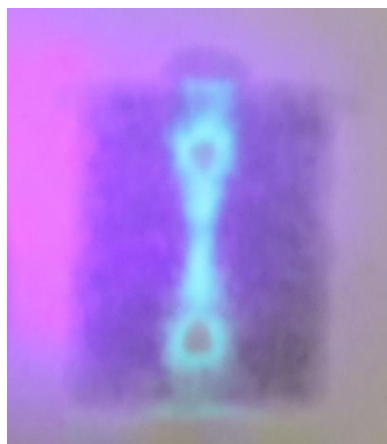


Figure 13 Contact angle 20 layers of ink a) Whatman n°1; b) Supor pore 200 by Pall Company

With this equipment it is possible to visualise in real time the interaction of the liquid drop with the substrate and by using its software allow to calculate the contact angle. This calculation is based on the Young equation (5).

After 10 min with the solution on top it was observed Figure 13 this time was used to ensure that liquid would be absorbed by the samples. The contact angle obtained in the papers was 47.2° for the Whatman and 51.5° for supor pore 200. This means that ink is does not show a hydrophobic behave since there is some spreading. Due to the nature of the ink being a UV curable polymer this is crosslinking and forming an impermeable barrier.

After this step, a flux test was performed to ensure that the liquid could be contained inside the wells made for the sample. This is to be confirmed in the Figure 14 (the process was enhanced by using a food dye as well as UV light).



**Figure 14 Design and flux test of the microfluidic layer**

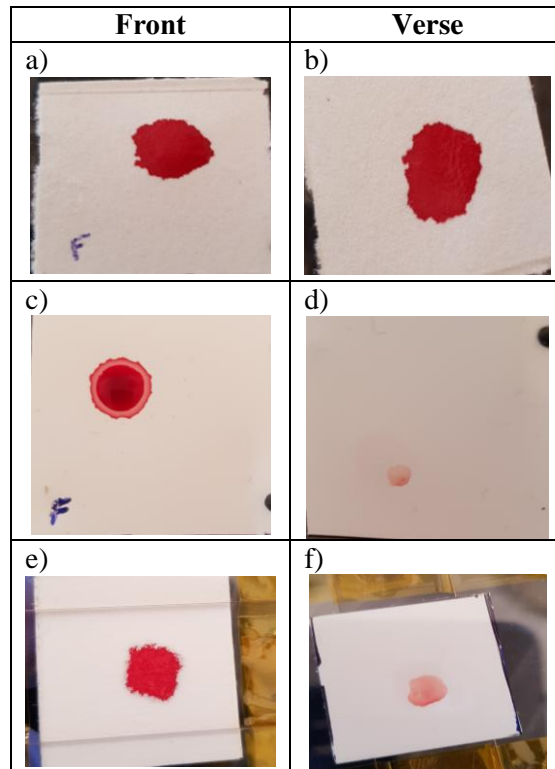
To improve the resolution and prevent unwanted spreading of the ink, a UV flashlight was mounted on the top of the printer during the printing process. Also, to ensure a better penetration of the ink in the paper substrate the stage was heated 60 °C. Although the liquid is mainly contained, there is some spreading and it's not hydrophobic for this reason other methods may be considered [55].

In this work, after considering the different types of paper, it was conclude that would be a better approach to use a 3D architecture of microfluidics devices, in order to obtain a filter able to contain the red blood cells and let the DNA pass through since it's only desired for the assay the DNA [55]. We indented to obtain such properties by combining two different types of paper. A first one that would act as a transport (Whatman n°1) and the second one that acts as a filter super pore 200 by Pall Company. The first paper used has a pore size of 11 µm what makes it useful to retain sample as well as work as transport layer. The second paper, the supor pore 200 has a pore size of 0.2 µm which makes it ideal to filter after the cellular lysis.

**Table II All blood composition**

Blood composition	size	ref
Red blood	6.2-8.2 µm	[56]
Platelets	2-3 µm	[57]
White blood cells	7 µm	[58]
Pair of nucleotide DNA	1nm	[59]
Unit	0.33 nm	[60]

Looking at the Table II, this would mean that if we could extract the DNA from the blood cells, the supor pore 200 would make possible filtering DNA from rest of the unwanted components. It was performed a test with a real blood sample in order to see the filtering process.



**Figure 15** Sample of Whatman n° 1 pore size 10  $\mu\text{m}$  - a) and b); Supor pore 200 pore size 0.2  $\mu\text{m}$  - c) and d); Sandwich assay using the Whatman n°1 on top and the Supor pore 200 below – e) and f)

With the assay presented in Figure 15, it was possible to see a separation between the blood composition. It is possible to verify a strong reddish colour in the samples using the Whatman and in the front side of the Supor pore 200 leading to believe that, in fact, the red blood cells were actually filtered a), b) and c).

### 3.2. Resistance /Heat

As it is possible to observe in annex 2 and 3 the fabrication of features of 5 and 2  $\mu\text{m}$  was every difficult to achieve using this fabrication methods. Also, we need to have in consideration the high aspect ratio and for this reason in-between the images shown in annex 2 and the ones presented in annex 3, the process was changed. This time instead of drying the samples after the development with a stream of nitrogen (which seems most likely the reason to cause de defects observed in annex 2) the samples were dried by quickly put them in the spin coater and applying a high rotation followed by a quick heating to evaporate some humidity. This allow us to pass through the problems presented in annex 1 and obtain the images presented in annex 3.

For this reason, it was decided to use a mask with features of 50  $\mu\text{m}$  and 10  $\mu\text{m}$  and even though the features of 10  $\mu\text{m}$  were very hard to obtain, since most of the time the lines were disrupted (annex 6). Thus, the results presented were focused in the devices with the features of 50  $\mu\text{m}$ .

As explained in the previous chapters, the resistance measurements were obtained with the use of a cascade probe station. For purpose of simplicity it was attributed to each line a code, as it can be seen in the Figure 16.



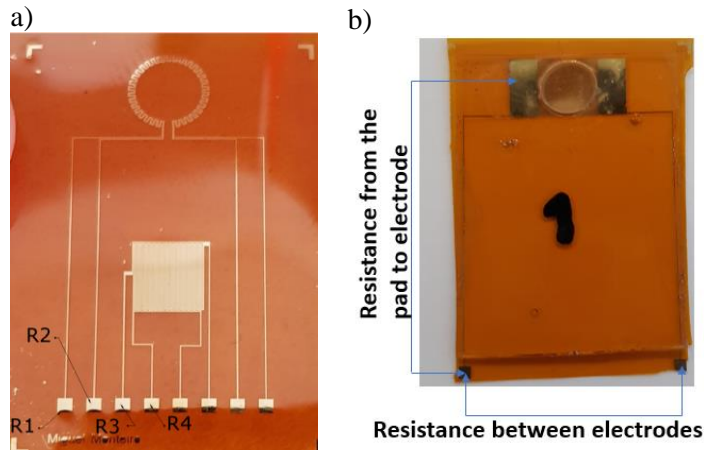


Figure 16 a) Resistance layer; b) Resistance measured in the capacitor

The first resistance (R1) is the thermocycler, the second resistance (R2) is the thermo sensor to control the temperature in the thermocycler, the third resistance (R3) will act as thermolysis method for the sample and fourth resistance (R4) will be a sensor to control resistance R3.

On the example of the Figure 16, an IV sweep was performed to obtain the measurements as shown in the following graphic:

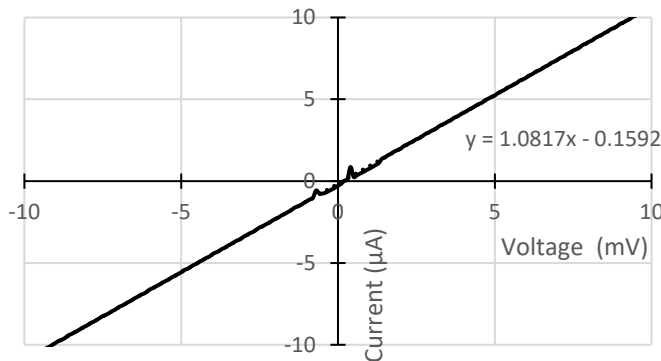


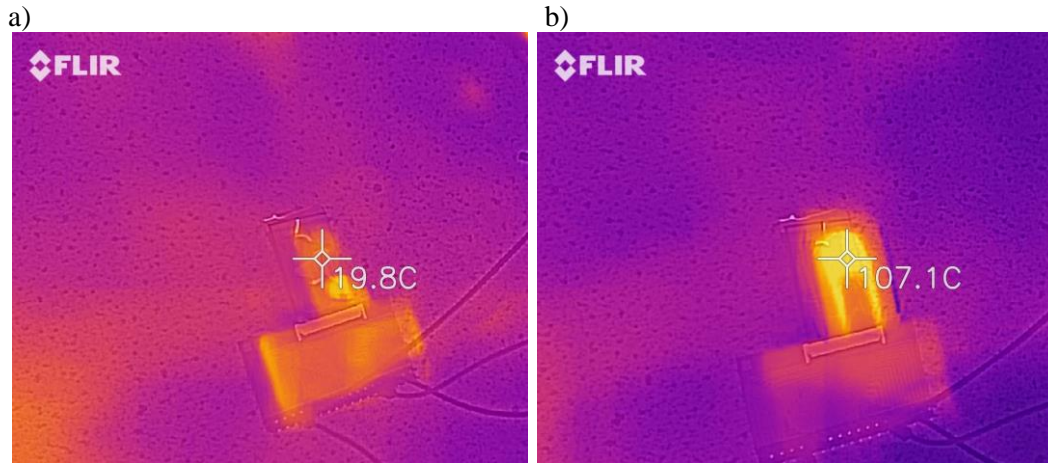
Figure 17 Example of the IV sweep taken to characterise the resistances

Table III Average values of the resistances presented in Figure 16

R1	R2
1.02 K $\Omega$ $\pm$ 0.07	1.01 K $\Omega$ $\pm$ 0.02
R3	R4
1.63 K $\Omega$ $\pm$ 0.11	1.48 K $\Omega$ $\pm$ 0.15
Resistance from the pad to electrode	Resistance between electrodes
571 $\Omega$	3.97 $\times$ 10 <sup>10</sup> $\Omega$

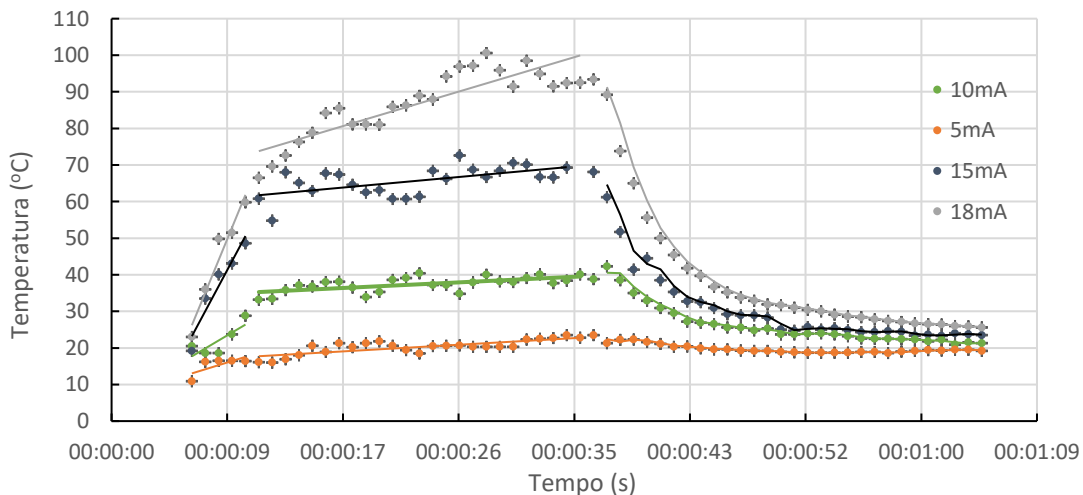
Based on this information we could easily obtain the resistance value by considering the slope of the line since this is an IV measurement as shown in Figure 17. The result of V/I by the Ohm law equals the resistance. The resistance was obtained using the trend line and taking out the slope value. The Table III presents the average values of the resistances.

With this method it was also possible to observe a resistance between the electrodes and the pads, to ensure that the lines were not cut. Also, the resistance between electrodes was measured and as expected, it was in the order of 10<sup>10</sup>  $\Omega$ , which means that the circuit was open as pretended. In order to facilitate this study, and to make it closer to a final product, it was designed and ordered a PCB which was weld to the ZIF connector.



**Figure 18** Thermo image of the resistances before and after applying current through the resistance a) Room temperature; b) After applying current

Once the montage was finished and the PCB was connected to a power source, was then possible to retrieve the images in Figure 18. The images were collected using a thermal camera and recoding the heating and cooling behaviour of the micro heaters, transduced in the following graphic:



**Figure 19** Thermocycler the increase of temperature for each current with and error of 0.1°

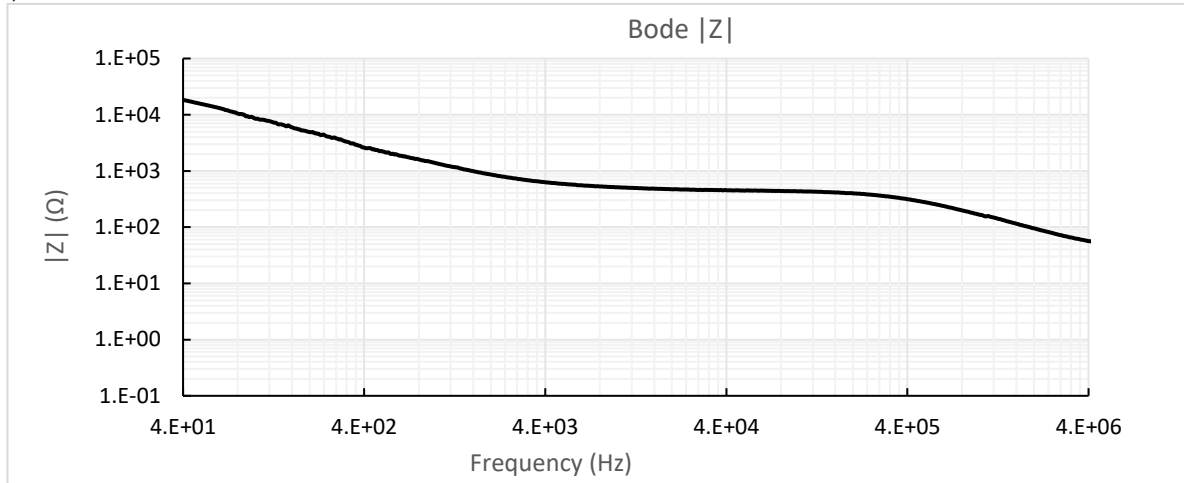
Observing the graphics in Figure 19, it is clearly noticeable that resistances are acting as expected from a thermocycler with quick heating ramps and a slower but still a reasonable cooling behaviour. Used in parallel with the sensor line and with software would be possible to obtain a graphic as the one represented in Figure 2 c).

Thermolysis has shown potential in becoming more common in large scale production. Thermolysis trigger the breakdown of cell walls and membranes at minimum of 85°C in a water bath for 20–30 min. Improved protein release has been obtained after short high thermal shocks, which increases the process efficiency and decreases the necessary time for the complete lysis. [61].

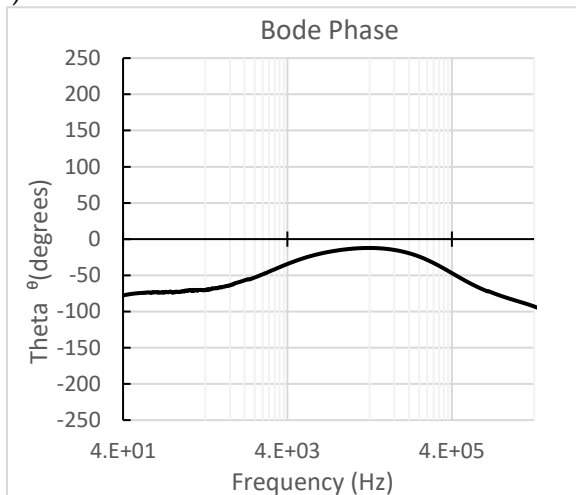
### 3.3. Impedance

As mentioned in the previous chapters this data was collected using a cascade probe station, connected to an Impedance Spectroscopy Analyser and we were able to gather the following results:

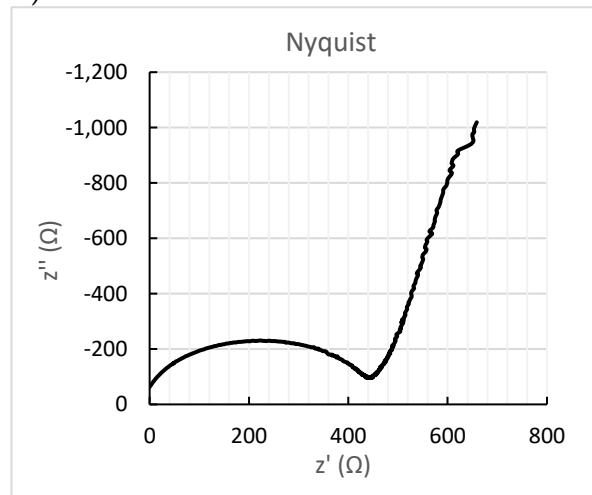
a)



c)



d)



**Figure 20 Different plots obtained by impedance spectroscopy**

The graphics presented in the Figure 20 resulted from the measurements between the pads of the device with the SU8 well filled up with a PBS solution, in order to mimic the medium where the electrode will be working and avoiding the alteration in the behaviour not caused by the hybridisation event.

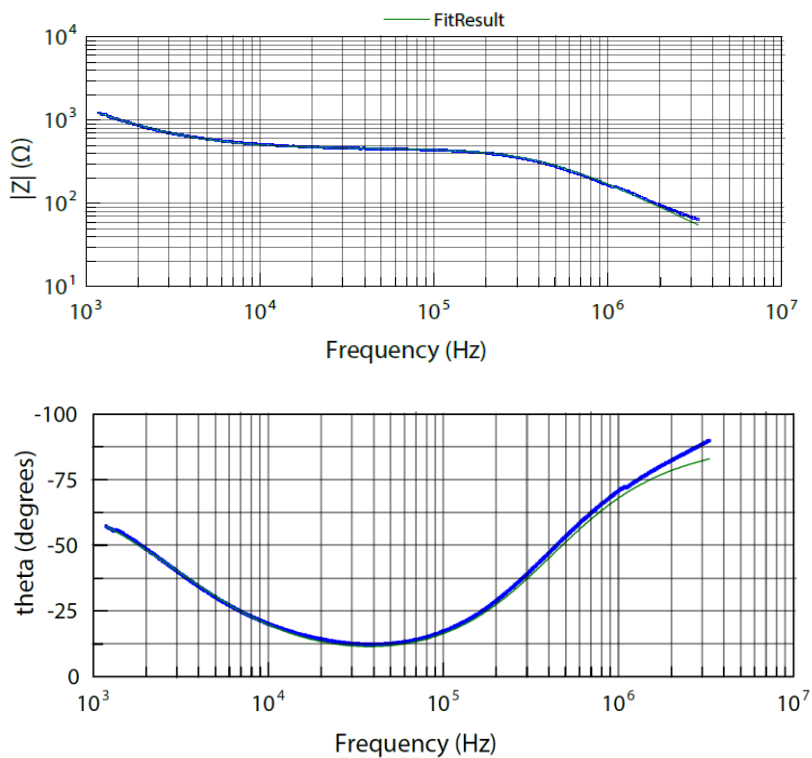
It is possible to observe in Figure 20 a), that our capacitor magnitude starts with a slope which is a very typical behaviour expected from a commercial capacitor as presented in annex 8. However, the regime disappears for frequencies of  $5 \times 10^4$  Hz and it became a constant line, a typical resistance behaviour due to the electrolyte relaxation. Even though, with higher frequencies it is possible to perceive a capacitive regime again.

In Figure 20 b), it is possible to observe that in lower frequencies shows a  $-90^\circ$  degrees of phase, a typical behaviour of a capacitor. At the same frequency  $5 \times 10^4$  Hz but in  $-45^\circ$  degrees (which represents the inversion of behaviour) the capacitor passes to a resistance phase with  $0^\circ$  degrees.

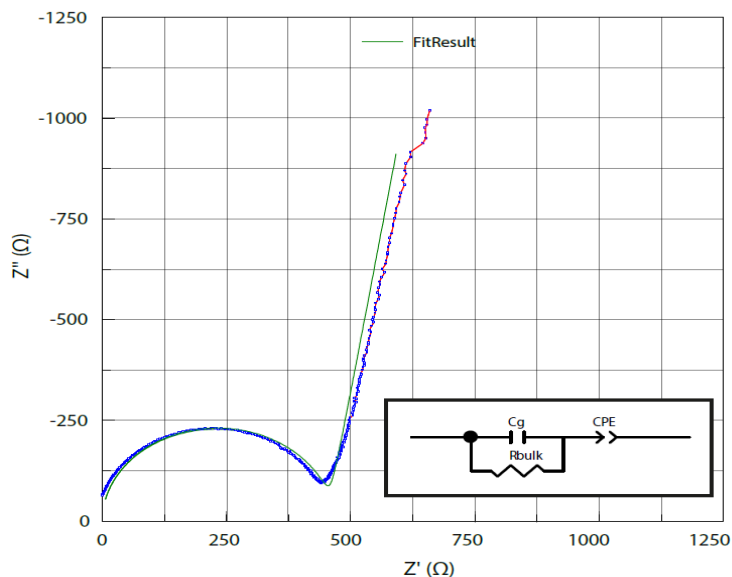
In conclusion, this type of changes is not typical of a commercial capacitor but are very known in electrolyte capacitors with electrochemistry in play.

With these previous results, it is possible to perform a fitting model with *Zview* software from *Scribner* company as shown in the Figure 21.

a)



b)



<u>Element</u>	<u>Freedom</u>	<u>Value</u>	<u>Error</u>	<u>Error %</u>
Cg	Free(+)	8.78E-10	2.83E-12	0.322
Rbulk	Free(±)	451	1.01	0.223
CPE-T	Free(+)	3.03E-07	1.36E-08	3.24
CPE-P	Free(+)	0.903	0.003	0.384

**Figure 21** Equivalent model and fitting a) Bode diagram b) Nyquist

Where  $C_g$  is the capacity caused by the geometry of the capacitor,  $R_{bulk}$  is the resistance associated to pads to electrodes CPE is a constant phase element where CPE-T is a pseudo capacitance which is called Q, CPE-P is related to the semi-circle in nyquist plot (depressed semicircle), normally used the notation  $n$ . [62]

According to these values it is possible to observe a high value of  $n$ , that permits to approximate the CPE to a capacitor with value of  $3.03 \times 10^{-7}$  F resulted from the double layer effect. Although the value of the double-layer capacitance depends on many variables including electrode potential, temperature, ionic concentrations, types of ions, oxide layers, electrode roughness, impurity adsorption for example.

As we can see this model gives a good fitting to what is obtain in the experimental process it is necessary to perform further studies and new assays

It is expected to see similar behaviour in the capacitor when functionalized and with hybridisation process as shown in Figure 11 and with equivalent circuit shown in Figure 5, in this case the electronic components would represent:

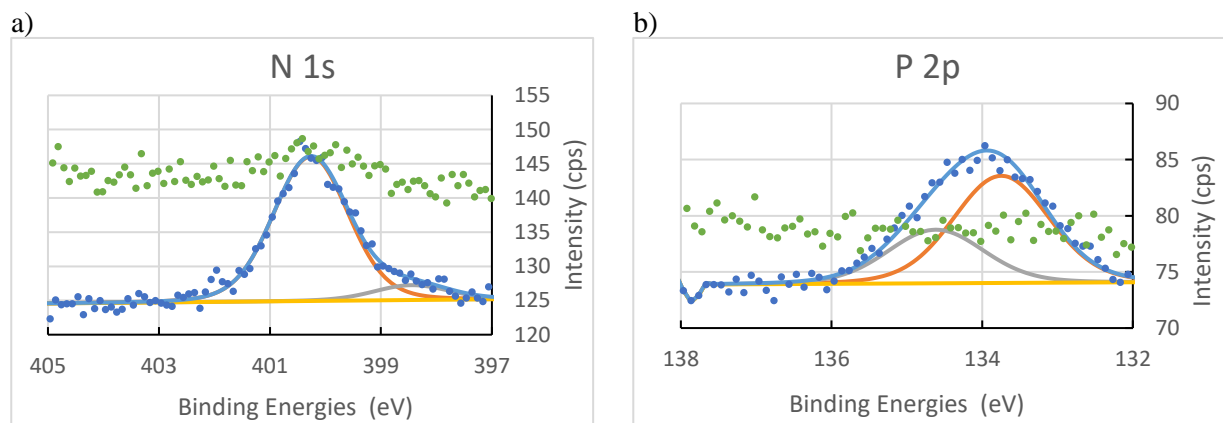
With a  $R_s$  solution resistance which is determined by the ion concentration and the cell geometry, the double-layer capacitance ( $C_{dl}$ ) is given by the charge stored in the double layer at the interface also dependent on the electrolyte and the charge transfer resistance ( $R_{ct}$ ) originates from chemical reactions at the electrode or impurities accumulated on its surface. The impedance of the biological material in a sensor arrangement, that were immobilized on top of the working electrode will cause changes in of components  $R_{ct}$  and  $C_{dl}$  of the electrode. This behaviour is similar to the one presented in Figure 20 and 21, nonetheless we conclude that it is not what is shown in this figures, due to the frequency ranges and also the fact that these measurements were taken before the functionalization step, so we would not have a  $R_{ct}$  because there is nothing attached to the golden surface.

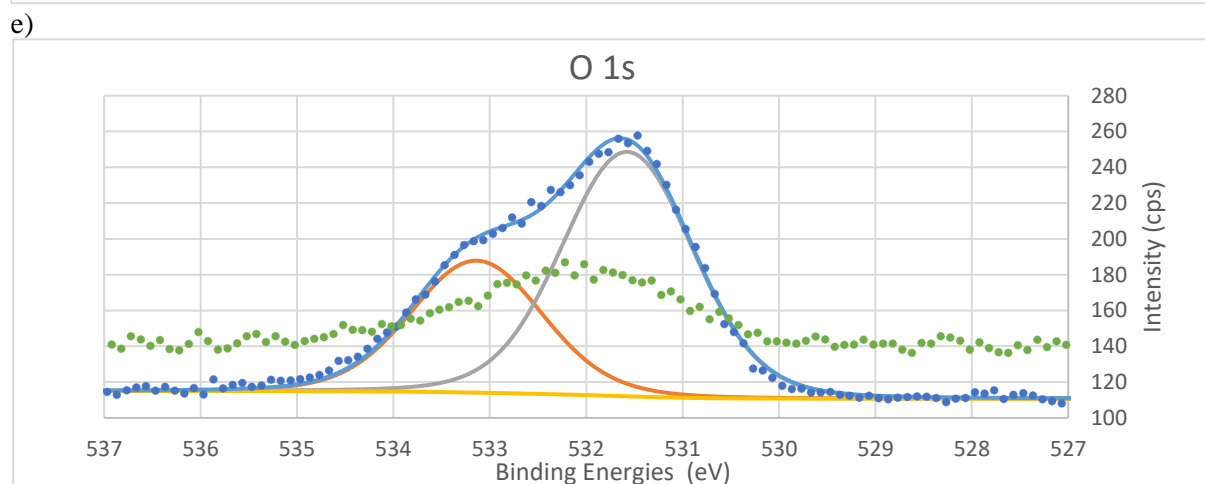
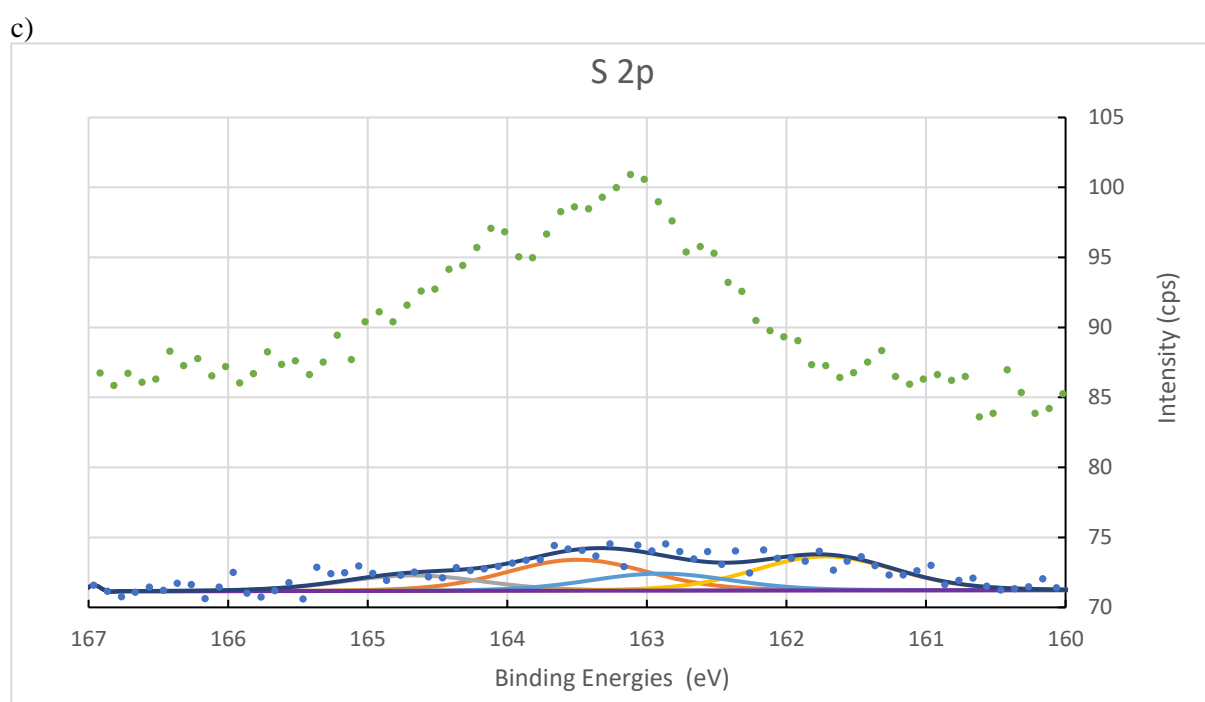
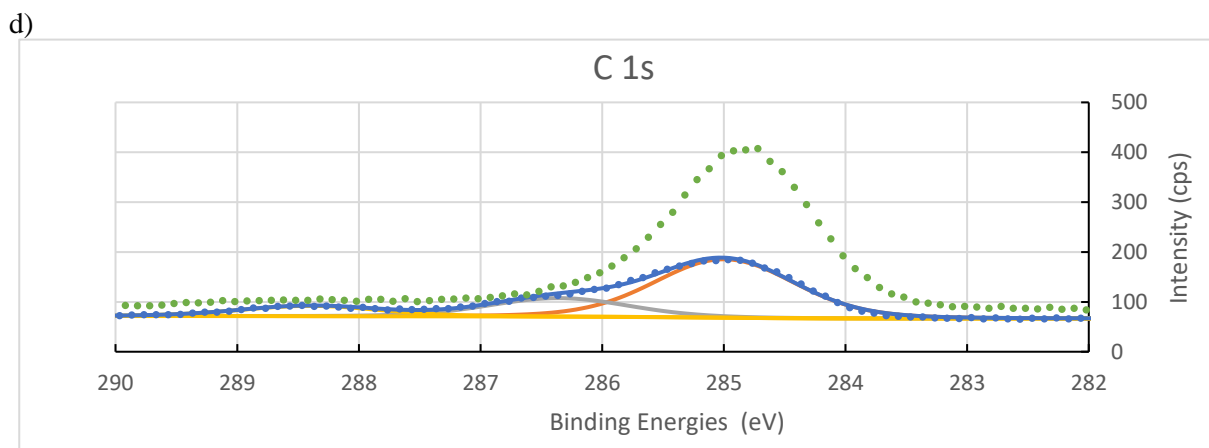
When analyzing the data retrieved from RT-qPCR cycles let us to believe that there were some measurements errors (shown in annex 9). With some other assays (shown in annex 10 and 11) we conclude that the problems presented were caused by the reading equipment and not by the fabrication of the device.

As in the time window of this project there was no way to repair the equipment we used a second method to ensure that the functionalization step was successful.

### 3.4.X-ray photoelectron spectroscopy (XPS)

As a second method to confirm that the functionalisation step was successful it was necessary used the XPS technique since it let us know what chemical elements are on the top of the electrodes golden surface. XPS spectra are obtained by irradiating a material with a beam of X-rays while simultaneously measuring the kinetic energy and number of electrons that escape from the top 0 to 10 nm of the material being analysed. The XPS spectroscopy survey spectra is presented in Figure 34 (annex 12).





**Figure 22 Shows the XPS spectra of each chemical element were the points in blue represent a sample functionalized with SAM and dsDNA and the green points is a sample where it was removed the DNA with respective fitting adjustments (N – Nitrogen, C – Carbon, S – Sulfur, P – Phosphor, O – Oxygen).**

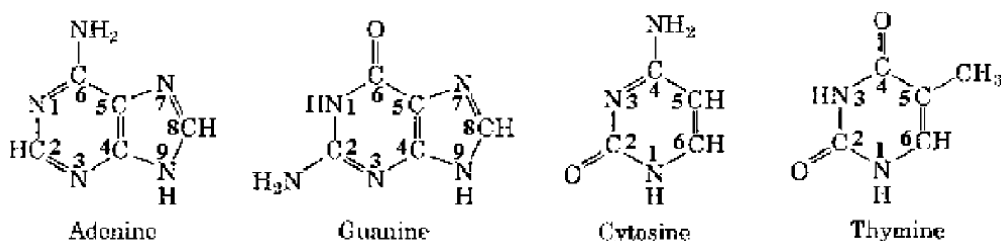
The Figure 22 represents an X-ray photoelectron spectroscopy of two different samples, the blue contains DNA and the green surfer from a previous UV ozone cleaning step to eliminate the DNA.

The green sample works as a control to better understand the DNA influence in the X- Ray spectre of both measurements. It is also important to underline the lower peak intensity of P 2p (Figure 22 b)) in the green sample compared to the blue one, which is justified by the DNA backbone. In Figure 22 c) it was verified a raise in the peak intensity explained by absence of the DNA resulted by UV ozone clean process. Nevertheless, the thiol groups bonded to the gold were not removed during this process, which led to a more direct exposition to the X-ray beam and consequently the increase of the peak intensity.

The differences of the measurements in both samples are also traduced in Table IV.

**Table IV Distribution and concertation of elements in the samples**

Elements	Blue sample				Green sample		
	Position	Raw Area	%At Conc		Position	Raw Area	%At Conc
O 1s	531.47	374.232	32.03		532.22	113.444	7.36
N 1s	400.47	41.0389	5.52		400.42	4.60866	0.47
C 1s	284.97	259.843	58.55		284.72	528.443	89.65
S 2p	163.27	9.68019	0.89		163.12	30.8526	2.08
P 2p	133.97	23.8725	3.02		132.52	4.86179	0.45



**Figure 23 Nucleotides structure adapted from [60].**

With the graphics obtained by the XPS using the blue dots sample we were able to produce the Table V:

Table V shows a possible decomposition of the XPS spectra with binding energies collected from the graphics in the Figure 22

Orbital	Position	Binding Energies (BE) (eV)	Reference values [32], [60–62]	Chemical bonds
O 1s	1	531.57	531.1	C-O-C cyclic ether (deoxyribose); N-(CO)-X (X = C or N) (bases)
	2	533.14	532-534	PO <sub>4</sub> <sup>-</sup> (backbone)
N 1s	1	398.45	398.8	-N= conjugated
	2	400.26	399.9-401.0	-NH <sub>2</sub> > N- (in C and A); N-(CO)-N (T)
C 1s	1	284.99	284.7-286.2	-C-C- (deoxyribose); -C= (C5 in C); -CH (alkyl chain -C <sub>3</sub> SH, methylgroup in T and aliphatic contamination); (CO)-C= (C5 in T)
	2	286.35	286.0-287.0	C-N and N-C=N (A and C6 in C and T); C-O-C cyclic ether (deoxyribose); -CH <sub>2</sub> -O- (sugarsphosphate bond)
	3	288.4	287.8-289.1	C-NH <sub>2</sub> (C6 in A and C4 in C); N-(CO)-C (C4 in T); N-(CO)-N (C2 in C and T)
S 2p	1	161.72	161.9	S-Au
	2	162.9	163	
	3	163.5	163.5	Thiol-S
	4	164.68	164	
P 2p	1	133.75	133.9-134.2	-PO <sub>4</sub> <sup>-</sup> (backbone)
	2	134.62	+0.87	

Comparing the values of the binding energies with the ones reported in the literature, we can extrapolate and try to identify what those energies are related with. In order to analyze these values, first it must be considered that the DNA molecule is a sensitive biological target upon exposure to ionizing radiation.

C 1s, N1s, O1s and P 2p XPS spectra variation of DNA are reported to occur just after 1h of exposure to X-ray beam [66]. Although, in the paper where is reported this variation in the DNA spectra the XPS method used does not include a monochromator while the one presented in this study does. The use of the monochromator makes the intensity of the beam significantly less intense. Also, in the specific case of carbon is possible that the sample could be contaminated, so the C 1s spectra must be considered with care. Figure 22 b) shows the evolution of the C 1s spectra. Due to charge accumulation it was used a conventional method where we adjusted the binding energy of the bond C-C to a reported value for this effect the C 1s was calibrated to the value 285 eV and used to adjust the other elements values. From literature was being observed that energies in ranges of 284.7-286.2 eV that can be associated with carbons in the nucleotides structure. Being the first range for a peak 284.7-286. eV which is associated with -C-C- bond in (deoxyribose), -C= (C5 in C) and the (CO)-C= (C5 in T). The second peak between 2286.0-287.0 eV that could be related with C-N and N-C=N (A and C6 in C and T) and C-O-C cyclic ether (deoxyribose). And the third one between 287.8-289.1 eV which could be caused by C-NH<sub>2</sub> (C6 in A and C4 in C), N-(CO)-C (C4 in T) and N-(CO)-N (C2 in C and T). The Figure 23 as the chemical structure and the numeration of carbons.

Even though N element is also damaged by X-ray, it is known to be quite robust against surface contamination during sample preparation and handling. Thus, its existence may indeed indicate adsorption of the DNA sample onto the substrate.

The N 1s signal from the surface is reported in Figure 22 a) and has a binding energy distribution between 403.0 and 399.0 eV, consistent with published results for other DNA samples. Similar results have been reported by A. Opdahl, in reference "*Independent control of grafting density and conformation of single-stranded DNA brushes*" [64]. where synthetic ssDNAs containing a controlled number of Adenine and Thymine chains were anchored selectively to a gold surface. In this paper where reported a single peak at 401 eV BE for dT, and the second peaks at 399 eV BE for dA. Looking at the results obtained in this study we can see two peaks at these two regions and a more intense peak in the region of the 401 eV. According to literature this would mean that we have a more Thymine than Adenine. Since the XPS was performed on a sample that only passed through the functionalisation step the only DNA presented in the sample is the one bind to the thiol groups. Looking to the sequence of the YWHAZ primers it is confirmed the number of Thymine bigger than Adenine which suggests that the functionalisation step was well succeeded.

In the S 2p spectra it is possible to observe two types of behaviour. According with the literature the binding energy of sulfur to gold when these forms a covalent bond is 161.9 eV and a second spike at 163 eV as for the unbound thiols they have energies between 163.5 and 164 eV [65]. Although this graphic had low intensity and presented a lot of noise, this can be caused by the fact that the sulfur is bonded to the golden surface making it lower than the rest of the elements. Keeping in mind that the XPS only have a range of 10nm deepness this can provide an explication to the noise presented in graphic.

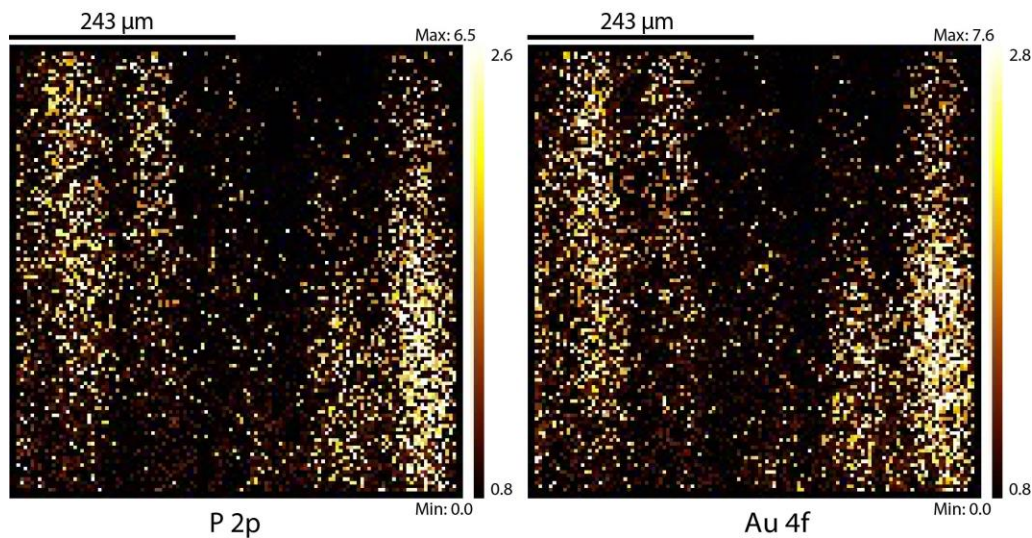
The phosphor element it is characteristic of a backbone in the DNA structure so looking at P 2p spectra we can see an energy between 133.9-134.2 that is reposted as being associated with the DNA structure.



**Table VI Chemical list**

Chemical	Linear Formula
3-MPA	HSCH <sub>2</sub> CH <sub>2</sub> COH
16-Mercaptohexadecanoic acid	HS(CH <sub>2</sub> ) <sub>15</sub> CO <sub>2</sub> H
Tris-hydroxymethyl-aminoethane	NH <sub>2</sub> C(CH <sub>2</sub> OH) <sub>3</sub>
EDC N-(3-Dimethylaminopropyl)-N'-ethylcarbodiimide hydrochloride	C <sub>8</sub> H <sub>17</sub> N <sub>3</sub> · HCl
Sulfo- NHS N-Hydroxysulfosuccinimide sodium salt	C <sub>4</sub> H <sub>4</sub> NNaO <sub>6</sub> S
Ethanolamine	NH <sub>2</sub> CH <sub>2</sub> CH <sub>2</sub> OH
BSA	CH <sub>3</sub> C[=NSi(CH <sub>3</sub> ) <sub>3</sub> ]OSi(CH <sub>3</sub> ) <sub>3</sub>

Looking at the chemical's we can also see that the P element its not present in any other compost of the solutions involved in the process. This led to believe that if there is any phosphor it must be from the DNA probes anchored with the thiol groups since the samples were washed and dried briefly in a stream of nitrogen.



**Figure 24** In this image it is shown the distribution of the elements in sample.

Therefore, it was possible to produce the images presented in Figure 24 with distribution of the P and Au elements in the sample. We can see the mapping of the chemical elements and as expected there is an overlapped. The images also show that the elements form this kind of stripes, which are the fingers of the capacitor.



## **4. Conclusion**

As anticipated, the main goal of this work is to design, develop and optimize the fabrication process of a biosensor, towards the design and development of a fully functional POCD biosystem capable to perform a full qPCR-based assay, starting from the whole biological sample (e.g. blood), to the extraction of the DNA from the red blood cells by thermolysis, its biofiltration through the paper filter and transport layer, mixing with primers and probes to isolate the targeted amplicons, their amplification and detection, performed in the capacitive biosensor and thermocycler sections.

Although preliminary, this study shows that it is possible to obtain an adequate thermocycler to achieve a fast and precise temperature control. Also, we can realise that, with further developments, it is possible to obtain a 3D microfluidic structure, acting as a transport layer and biofilter. On the other hand, for the capacitive biosensor layer, the results obtained in this work, point into the direction of a viable option for replacing all additional process steps required for sample preparation, fluorescence detection and data processing commonly performed in specialised laboratories performing qPCR-based assays. At this stage though the measurements were affected by considerable noise, which means that we cannot conclude whether the impedance changes observed and reported in the characterisation graphics are due to hybridisation and amplification events or not. This noise is most likely caused by the specific electrical probes used to take the measurements. In fact, we could observe the same source of noise when we try to measure a commercial SMD capacitor, in a control experiment, as reported in annex 10.

Upon removing the source of noise, it is expected that the hybridisation events and the qPCR amplification cycles would produce a shift to lower frequencies of the impedance peak, related to the negative charges associated with the phosphate group of the DNA. This would cause a negative charge in both electrodes, which would may cause a delay in the charge of the capacitor and for the same reason a shift of the bell-shaped graphic toward lower frequencies. Another important aspect to consider in further studies is the device sensitivity that could explain the very low changes in impedance.

Nevertheless based on the results observed in contact angle we were able to fabricate a microfluidic prototype as well as a flexible Thermocycler with quick rapid heating ramps based on the images recovered from a thermo camera and finally a flexible base electrolyte capacitor that was further functionalized to with thiol groups and sDNA this results are shown by the impedance results and reinforced by XPS data analyze.



## ***5. Future perspectives***

Following the remarks presented in the previous chapter, it can be concluded that this area of investigation has a lot of factors that could have changed and altered the results. More work needs to be done, in order to optimize this technique and to bring this technology from the lab to the bedside of the patients. Some of this optimization process might involve:

- Use techniques to improve the Kapton surface smoothness to improve the process reliability;
- Do hybridisation test with negative control groups and blank control groups;
- Do a sensitivity test using known concentration of targeted DNA sequences;
- Use of nanofabrication tools as the e-beam lithography or nanoimprinting techniques, to allow smaller gaps between the fingers and therefore a more sensitive capacitor;
- Use of ion labels to improve sensitivity of the device;
- Use of single electrode functionalisation;
- Design of an array of electrodes for multiplex qPCR;
- More test studies and validation with real samples.

This work is the starting point toward further research and follow-on investigation aiming to be published in the near future by the same group at Cambridge University, in collaboration with Universidade Nova de Lisboa, as a full working biosensor for electric read out of RT-qPCR.

## References and Bibliography

- [1] S. K. Vashist, 'Point-of-care diagnostics: Recent advances and trends', *Biosensors*, vol. 7, no. 4, pp. 10–13, 2017.
- [2] M. Riedel, F. Lisdat, and G. Urban, 'Biosensorial Application of Impedance Spectroscopy with Focus on DNA Detection', in *Label-Free Biosensing: Advanced Materials, Devices and Applications*, M. J. Schöning and A. Poghossian, Eds. Cham: Springer International Publishing, 2018, pp. 133–178.
- [3] C. Stagni *et al.*, 'CMOS DNA sensor array with integrated A/D conversion based on label-free capacitance measurement', *IEEE J. Solid-State Circuits*, vol. 41, no. 12, pp. 2956–2963, 2006.
- [4] J. T. Connelly, J. P. Rolland, and G. M. Whitesides, "'Paper Machine" for Molecular Diagnostics', *Anal. Chem.*, vol. 87, no. 15, pp. 7595–7601, 2015.
- [5] S. Maddocks and R. Jenkins, *Understanding PCR : a practical bench-top guide*. 2017.
- [6] S. Yang and R. E. Rothman, 'PCR-based diagnostics for infectious diseases: Uses, limitations, and future applications in acute-care settings', *Lancet Infect. Dis.*, vol. 4, no. 6, pp. 337–348, 2004.
- [7] J. Chen and K. Li, 'Analysis of PCR Kinetics inside a Microfluidic DNA Amplification System', *Micromachines*, vol. 9, no. 2, p. 48, 2018.
- [8] B. G. Baldwin, 'Phylogenetic utility of the internal transcribed spacers of nuclear ribosomal DNA in plants: An example from the compositae', *Mol. Phylogenet. Evol.*, vol. 1, no. 1, pp. 3–16, 1992.
- [9] G. Moon and W. Shin, 'Establishment of Quantitative Analysis Method for Genetically Modified Maize Using a Reference Plasmid and Novel Primers', vol. 17, pp. 274–279, 2012.
- [10] L. Lin, L. Chamberlain, L. J. Zhu, and M. R. Green, 'Analysis of Gal4-directed transcription activation using Tra1 mutants selectively defective for interaction with Gal4', *Proc. Natl. Acad. Sci.*, vol. 109, no. 6, pp. 1997–2002, 2012.
- [11] I. M. Mackay, 'Real-time PCR in the microbiology laboratory', *Clin. Microbiol. Infect.*, vol. 10, no. 3, pp. 190–212, 2004.
- [12] L. Xi, D. G. Nicastri, T. El-Hefnawy, S. J. Hughes, J. D. Luketich, and T. E. Godfrey, 'Optimal markers for real-time quantitative reverse transcription PCR detection of circulating tumor cells from melanoma, breast, colon, esophageal, head and neck, and lung cancers', *Clin. Chem.*, vol. 53, no. 7, pp. 1206–1215, 2007.
- [13] S. A. Bustin, V. Benes, T. Nolan, and M. W. Pfaffl, 'Quantitative real-time RT-PCR - A perspective', *J. Mol. Endocrinol.*, vol. 34, no. 3, pp. 597–601, 2005.
- [14] M. A. A. Valones, R. L. Guimarães, L. A. C. Brandão, P. R. E. De Souza, A. De Albuquerque Tavares Carvalho, and S. Crovela, 'Principles and applications of polymerase chain reaction in medical diagnostic fields: A review', *Brazilian J. Microbiol.*, vol. 40, no. 1, pp. 1–11, 2009.
- [15] U. E. M. Gibson, C. A. Heid, and P. M. Williams, 'A novel method for real time quantitative RT-PCR.', *Genome Res.*, vol. 6, no. 10, pp. 995–1001, 1996.
- [16] 'Real-Time qRT-PCR'. [Online]. Available: <https://www.ncbi.nlm.nih.gov/probe/docs/techqpcr/>.
- [17] D. P. Nikolelis and G. P. Nikoleli, *Nanotechnology and Biosensors*. Elsevier Science, 2018.
- [18] Z. Altintas, *Biosensors and Nanotechnology: Applications in Health Care Diagnostics*. Wiley,

2017.

- [19] J. Y. Yoon, *Introduction to Biosensors: From Electric Circuits to Immunosensors*. Springer International Publishing, 2016.
- [20] C. Berggren, P. Stålhandske, J. Brundell, and G. Johansson, 'A feasibility study of a capacitive biosensor for direct detection of DNA hybridization', *Electroanalysis*, vol. 11, no. 3, pp. 156–160, 1999.
- [21] V. Tsouti, C. Boutopoulos, I. Zergioti, and S. Chatzandroulis, 'Capacitive microsystems for biological sensing', *Biosens. Bioelectron.*, vol. 27, no. 1, pp. 1–11, 2011.
- [22] M. A. Parashchenko, S. Member, N. S. Filippov, N. V. Vandisheva, V. V. Kirienko, and S. I. Romanov, 'Capacitance Sensor with Nanoporous Insulator for PCR Detection', pp. 44–46, 2009.
- [23] R. Igreja and C. J. Dias, 'Analytical evaluation of the interdigital electrodes capacitance for a multi-layered structure', *Sensors Actuators, A Phys.*, vol. 112, no. 2–3, pp. 291–301, 2004.
- [24] S. Grimnes and O. G. Martinsen, *Bioimpedance and Bioelectricity Basics*. Elsevier Science, 2014.
- [25] M. E. Orazem and B. Tribollet, *Electrochemical Impedance Spectroscopy*, vol. 48. 2008.
- [26] J. F. Rubinson and Y. P. Kayinamura, 'Charge transport in conducting polymers: Insights from impedance spectroscopy', *Chem. Soc. Rev.*, vol. 38, no. 12, pp. 3339–3347, 2009.
- [27] M. J. Schöning and A. Poghossian, *Label-Free Biosensing: Advanced Materials, Devices and Applications*. Springer International Publishing, 2018.
- [28] A. Kukol, P. Li, P. Estrela, P. Ko-Ferrigno, and P. Migliorato, 'Label-free electrical detection of DNA hybridization for the example of influenza virus gene sequences', *Anal. Biochem.*, vol. 374, no. 1, pp. 143–153, 2008.
- [29] Ghafar-Zadeh and M. Sawan, *CMOS Capacitive Sensors for Lab-on-Chip Applications*. 2010.
- [30] C. Silva Martin, M. Dassi Maximino, M. Santos Pereira, C. de Almeida Olivati, and P. Alessio, 'The role of film composition and nanostructuring on the polyphenol sensor performance', *AIMS Mater. Sci.*, vol. 4, no. 1, pp. 27–42, 2016.
- [31] J. Bisquert, G. Garcia-Belmonte, P. Bueno, E. Longo, and L. O. S. Bulhões, 'Impedance of constant phase element (CPE)-blocked diffusion in film electrodes', *J. Electroanal. Chem.*, vol. 452, no. 2, pp. 229–234, 1998.
- [32] C. Guiducci, C. Stagni, A. Fischetti, U. Mastromatteo, L. Benini, and B. Riccò, 'Microelectrodes on a silicon chip for label-free capacitive DNA sensing', *IEEE Sens. J.*, vol. 6, no. 5, pp. 1084–1092, 2006.
- [33] D. Mascolo *et al.*, 'Printed Functionalized Capacitors for Water-Induced Label-Free Detection of DNA Hybridization', *Sci. Adv. Mater.*, vol. 3, no. 3, pp. 496–514, 2011.
- [34] F. E. De Rothschild and D. U. Bochum, *Lecture notes.*, vol. 504, no. 7478. 2013.
- [35] H. S. Chuang and S. Wereley, 'Design, fabrication and characterization of a conducting PDMS for microheaters and temperature sensors', *J. Micromechanics Microengineering*, vol. 19, no. 4, 2009.
- [36] J. Wu, W. Cao, W. Wen, D. C. Chang, and P. Sheng, 'Polydimethylsiloxane microfluidic chip with integrated microheater and thermal sensor', *Biomicrofluidics*, vol. 3, no. 1, pp. 1–7, 2009.
- [37] A. K. Yetisen, M. S. Akram, and C. R. Lowe, 'Paper-based microfluidic point-of-care diagnostic devices', *Lab Chip*, vol. 13, no. 12, pp. 2210–2251, 2013.
- [38] J. Berthier, K. A. Brakke, E. Berthier, and S. Figure, *Open Microfluidics*, no. c. Wiley, 2016.
- [39] S. Figure, N. T. Nguyen, S. T. Wereley, and S. T. Wereley, *Fundamentals and Applications of*

- Microfluidics*, no. c. Artech House, 2002.
- [40] C. D. Chin, V. Linder, and S. K. Sia, ‘Commercialization of microfluidic point-of-care diagnostic devices’, *Lab Chip*, vol. 12, no. 12, pp. 2118–2134, 2012.
  - [41] M. Q. do N. Costa, ‘Desenvolvimento de Microfluídica em Papel para Utilização em Biossensores’, p. 99, 2012.
  - [42] X. Li, J. Tian, G. Garnier, and W. Shen, ‘Fabrication of paper-based microfluidic sensors by printing’, *Colloids Surfaces B Biointerfaces*, vol. 76, no. 2, pp. 564–570, 2010.
  - [43] O. Mhibik, S. Chénais, S. Forget, C. Defranoux, and S. Sanaur, ‘Inkjet-printed vertically-emitting solid-state organic lasers’, no. Umr 7538, pp. 1–8, 2016.
  - [44] E. Y. Bormashenko, *Physics of Wetting: Phenomena and Applications of Fluids on Surfaces*. De Gruyter, 2017.
  - [45] K. Mittal, *Advances in Contact Angle, Wettability and Adhesion*, vol. 2. 2015.
  - [46] P. Film, ‘DuPont Kapton HN™®’, vol. 5213.
  - [47] E. Macchia *et al.*, ‘Single-molecule detection with a millimetre-sized transistor’, *Nat. Commun.*, vol. 9, no. 1, p. 3223, 2018.
  - [48] Y. Yin and X. S. Zhao, ‘Kinetics and dynamics of DNA hybridization’, *Acc. Chem. Res.*, vol. 44, no. 11, pp. 1172–1181, 2011.
  - [49] T. Erkens, M. Van Poucke, J. Vandesompele, K. Goossens, A. Van Zeveren, and L. J. Peelman, ‘real-time RT-PCR data of porcine backfat and longissimus dorsi muscle , and evaluation with PPARGC1A’, vol. 8, pp. 1–8, 2006.
  - [50] N. Solanky, A. R. Jimenez, S. W. D. Souza, C. P. Sibley, and J. D. Glazier, ‘Expression of folate transporters in human placenta and implications for homocysteine metabolism’, *Placenta*, vol. 31, no. 2, pp. 134–143, 2010.
  - [51] N. Tommerup and H. Leffers, ‘Assignment of the Human Genes Encoding 14-3-3 Eta (YWHAH) to 22q12, 14-3-3 Zeta (YWHAZ) to 2p25.1–p25.2, and 14-3-3 Beta (YWHAB) to 20q13.1 byin SituHybridization’, *Genomics*, vol. 33, no. 1, pp. 149–150, 1996.
  - [52] Y. Nishimura *et al.*, ‘Overexpression of YWHAZ relates to tumor cell proliferation and malignant outcome of gastric carcinoma’, *British Journal of Cancer*, vol. 108, no. 6. pp. 1324–1331, Apr-2013.
  - [53] V. K. Weerasekara *et al.*, ‘Metabolic-Stress-Induced Rearrangement of the 14-3-3ζ Interactome Promotes Autophagy via a ULK1- and AMPK-Regulated 14-3-3ζ Interaction with Phosphorylated Atg9’, *Molecular and Cellular Biology*, vol. 34, no. 24. 1752 N St., N.W., Washington, DC, pp. 4379–4388, Dec-2014.
  - [54] R. Liang *et al.*, ‘Increased 14-3-3ζ expression in the multidrug-resistant leukemia cell line HL-60/VCR as compared to the parental line mediates cell growth and apoptosis in part through modification of gene expression’, *Acta Haematol.*, vol. 132, no. 2, pp. 177–186, 2014.
  - [55] L. Magro *et al.*, ‘Paper-based RNA detection and multiplexed analysis for Ebola virus diagnostics’, pp. 1–9, 2017.
  - [56] M. L. Turgeon, *Clinical Hematology: Theory and Procedures*. Lippincott Williams & Wilkins, 2005.
  - [57] B. Jean-michel, ‘Platelet Size in Man’, vol. 46, no. 3, pp. 321–337, 2018.
  - [58] A. K. Abbas, A. H. H. Lichtman, and S. Pillai, *Cellular and Molecular Immunology E-Book*. Elsevier Health Sciences, 2014.

- [59] J. D. Watson and F. H. C. Crick, ‘Molecular structure of nucleic acids’, *Nature*, vol. 171, no. 4356, pp. 737–738, 1953.
- [60] M. Mandelkern, J. G. Elias, D. Eden, and D. M. Crothers, ‘The dimensions of DNA in solution’, *J. Mol. Biol.*, vol. 152, no. 1, pp. 153–161, 1981.
- [61] Y. J. Zhang, S. Zhang, X. Z. Liu, H. A. Wen, and M. Wang, ‘A simple method of genomic DNA extraction suitable for analysis of bulk fungal strains’, *Lett. Appl. Microbiol.*, vol. 51, no. 1, pp. 114–118, 2010.
- [62] S. Dasgupta *et al.*, ‘Printed and electrochemically gated, high-mobility, inorganic oxide nanoparticle FETs and their suitability for high-frequency applications’, *Adv. Funct. Mater.*, vol. 22, no. 23, pp. 4909–4919, 2012.
- [63] M. R. Vilar *et al.*, ‘Interaction of self-assembled monolayers of DNA with electrons: HREELS and XPS studies’, *J. Phys. Chem. B*, vol. 112, no. 23, pp. 6957–6964, 2008.
- [64] A. Opdahl, D. Y. Petrovykh, H. Kimura-Suda, M. J. Tarlov, and L. J. Whitman, ‘Independent control of grafting density and conformation of single-stranded DNA brushes.’, *Proc. Natl. Acad. Sci. USA*, vol. 104, no. 1, pp. 9–14, 2007.
- [65] D. G. Castner, K. Hinds, and D. W. Grainger, ‘X-ray Photoelectron Spectroscopy Sulfur 2p Study of Organic Thiol and Disulfide Binding Interactions with Gold Surfaces’, *Langmuir*, vol. 12, no. 21, pp. 5083–5086, 1996.
- [66] S. Ptasińska, A. Styczyńska, T. Nixon, N. J. Mason, D. V. Klyachko, and L. Sanche, ‘X-ray induced damage in DNA monitored by X-ray photoelectron spectroscopy’, *J. Chem. Phys.*, vol. 129, no. 6, 2008.
- [67] C. J. Kaiser and S. Figure, *The Capacitor Handbook*, no. c. Springer Netherlands, 2012.

## Annex 1

The physics of the flows in microfluidic devices are governed by a transitional regime between the continuum and molecular-dominated regimes [39]. When analysing the physical properties of this micro systems it is very important to take in account the scale factors which express the variation of the physical quantities, according with the size of the system or the object in study, keeping quantities as pressure and temperature as constants. This way, it is possible to observe that some of the forces which usually have a bigger impact in macro scale like volume forces, at this scale they came to be less important while forces as surface tension and molecular interaction play a significant role [41].

According with Lucas-Washburn-Rideai (LWR), the hydrophobised filter paper samples can be strongly hydrophobic, and untreated cellulose has a contact angle of 25°. For porous materials which behave as a group of cylindrical capillaries, the equation that describes the penetrations of a liquid in time is:

$$l = \sqrt{\frac{\gamma r}{4\eta_v} t} \quad (6)$$

This way the penetration of a liquid in tube by capillary force is directly related to the radius of the capillary, to ratio between surface tension and viscosity is inversely proportional to the path filled by the liquid. This web of randomly disposed fibers allows some space between them (pours) so they act as small capillary tubes [41,42].

## Annex 2

After the development process and before going into the metallization step the samples were observed Figure 25 and the fingers with features of 5 and 2 μm.



**Figure 25 Az photoresist with 5 μm features after development**

This was the defects observed in the capacitors with the fingers with features of 5 and 2 μm



### Annex 3

After the eliminating the problems presented in annex 1 the sample went to the metallization and development process. After those it was possible to observe Figure 26

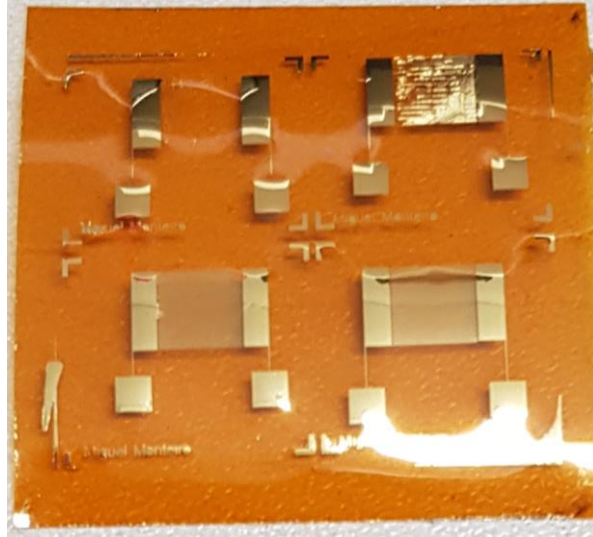


Figure 26 Capacitor features test

As it is shown in Figure 26 the capacitors with the features of 5 and 2  $\mu\text{m}$  when passing through the lift-off process the fingers disattached from the surface. And even the capacitors 10  $\mu\text{m}$  had low ratability being most of them shorted or with lines broken.

### Annex 4

First a thinner Kapton film was used in this work with a thickness of 25  $\mu\text{m}$ .

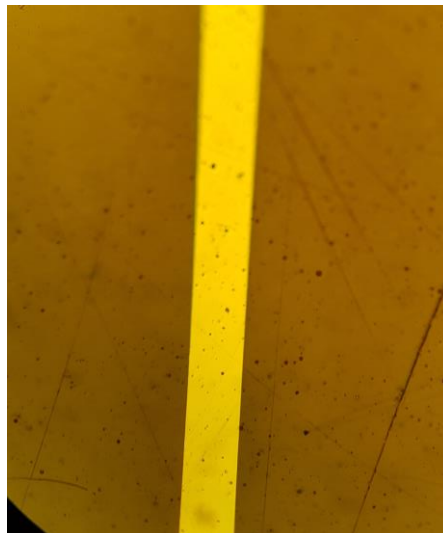
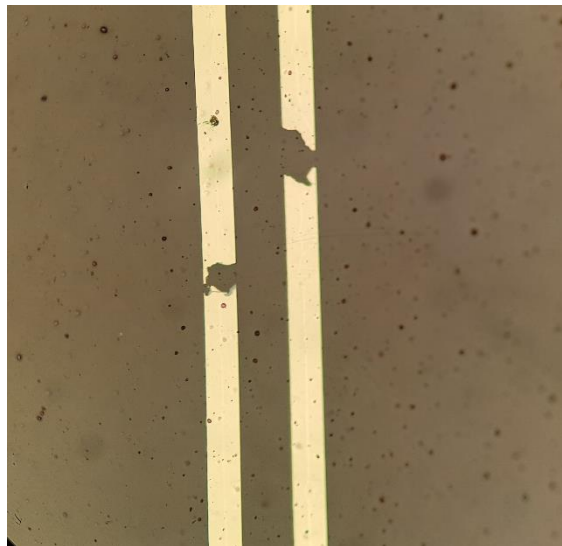


Figure 27 Sample of kapton with 25  $\mu\text{m}$

The Figure 27 is shown clearly a very scratchy surface which made the fabrication unfeasible since the scratches were to deep and as result it would end up with open circuit cases.

## Annex 5

Some defects that kept appearing

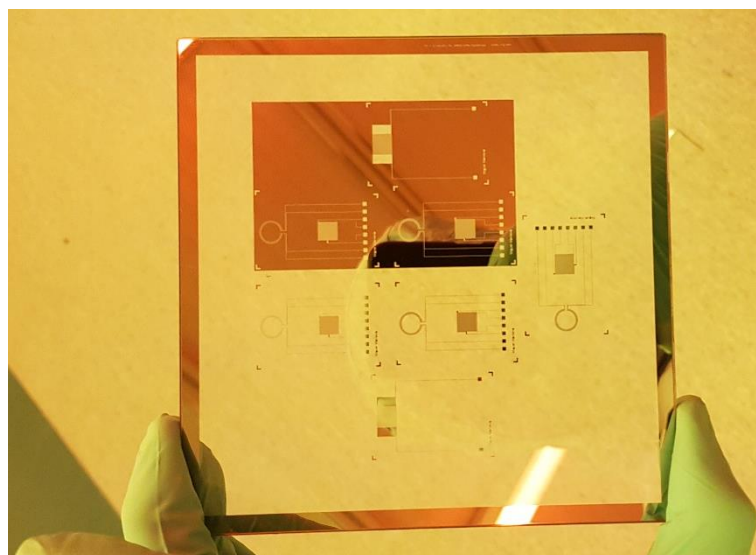


**Figure 28 Defects found on the devices after the fabrication step**

Looking at the defects in Figure 28 we can see this can be the result of impurities in the substrate or also could be cause during the lift-off process. To avoid them the substrate was further clean and left for a slow lift-off process overnight also the samples were left in a straight position for the golden pieces resulting of the lift-off process, would not be adsorbed to surface of substrate.

## Annex 6

Photolithographic mask for mask aligner 6'' design with *Autocad* and *Cleanwind* and order to JD photodata.



**Figure 29 JD mask**

This mask presented in Figure 29 was designed to have an area for reverse image and direct exposition

## Annex 7

The relation between the sample volume  $V$  and the analyte concentration  $A_i$  is given by:

$$V = \frac{1}{\eta_s N_A A_i} \quad (7)$$

where  $\eta_s$  is the sensor efficiency ( $0 \leq \eta_s \leq 1$ ),  $N_A$  is Avogadro number ( $6.02 \times 10^{23} \text{ mol}^{-1}$ ) and  $A_i$  is the concentration of analyte  $i$ . Equation (7) demonstrates that the sample volume or the size of the microfluidic device is determined by the concentration of the desired analyte [39].

## Annex 8

Impedance becomes a very useful consideration at higher frequencies because the capacitive effect disappears at certain frequencies, depending on capacitor design. The behaviour of practical capacitors with frequency resemble as the Figure 30. At the self-resonant point, in fact, they act entirely as a resistor.

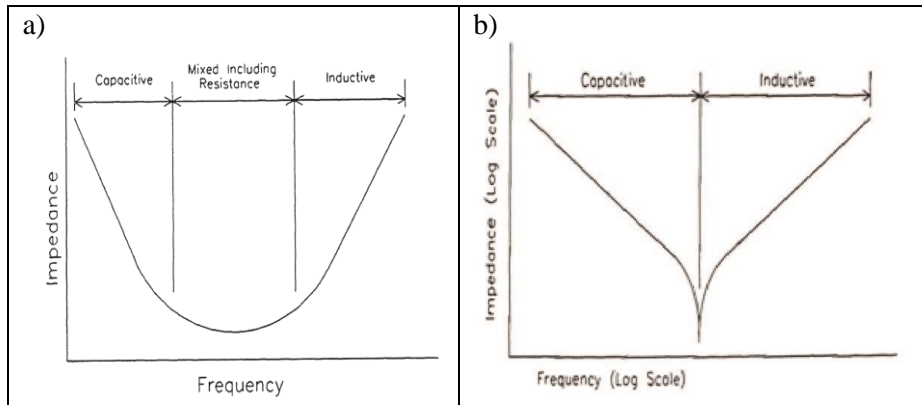


Figure 30 a) Typical behaviour of capacitor with Magnitude Vs Frequency a) linear scale, b) Log scale adapted from [27].

All capacitors look as a series circuit with all the three components: a passive resistance, inductance and capacitance as shown by equation:

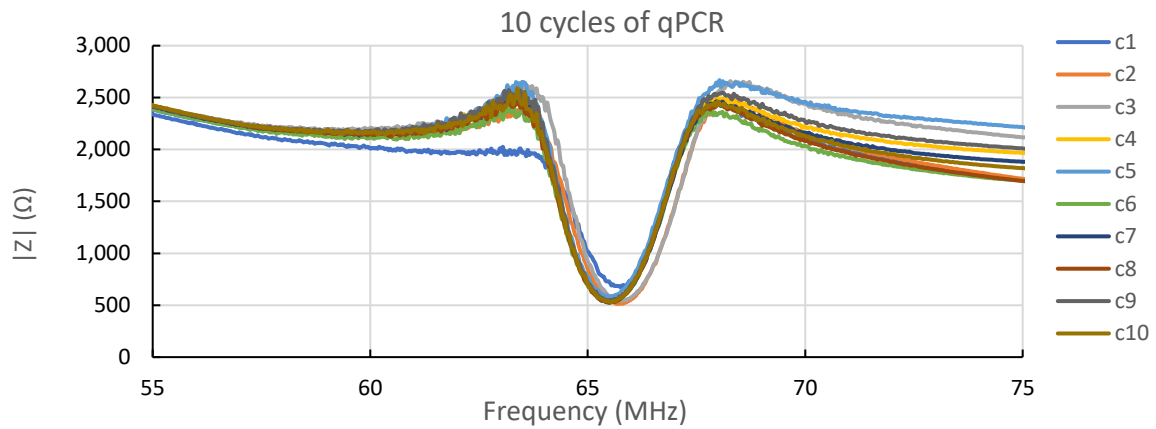
$$Z = \sqrt{R^2 + (X_L + X_C)^2} \quad (8)$$

Where  $Z$  is impedance,  $R$  is resistance associated with the resistive behaviour,  $X_L$  is resistance associated with the inductance behaviour,  $X_C$  is resistance associated with the capacitance behaviour.

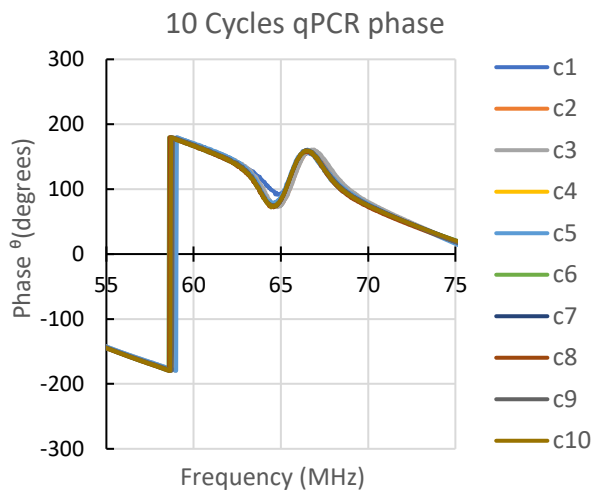
It should be reminded that,  $X_C$  decreases as frequency increases and also,  $X_L$  increases as frequency increases. Hence, capacitors are built with a very little inductance and a lot of capacitance, but if the frequency achieve a high enough value,  $X_C$  is eventually overtaken by  $X_L$  and the capacitive device now acts as an inductor [67].

## Annex 9

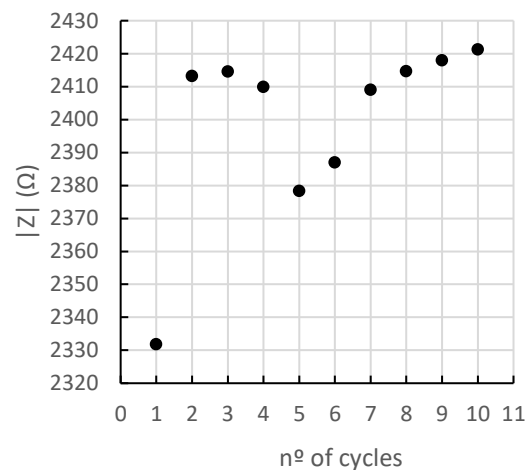
a)



b)



c)



**Figure 31 Impedance spectroscopy through the thermo cycling process a) Magnitude, b) Phase and c) how the impedance changes with nº o cycles for a frequency of 55 MHz**

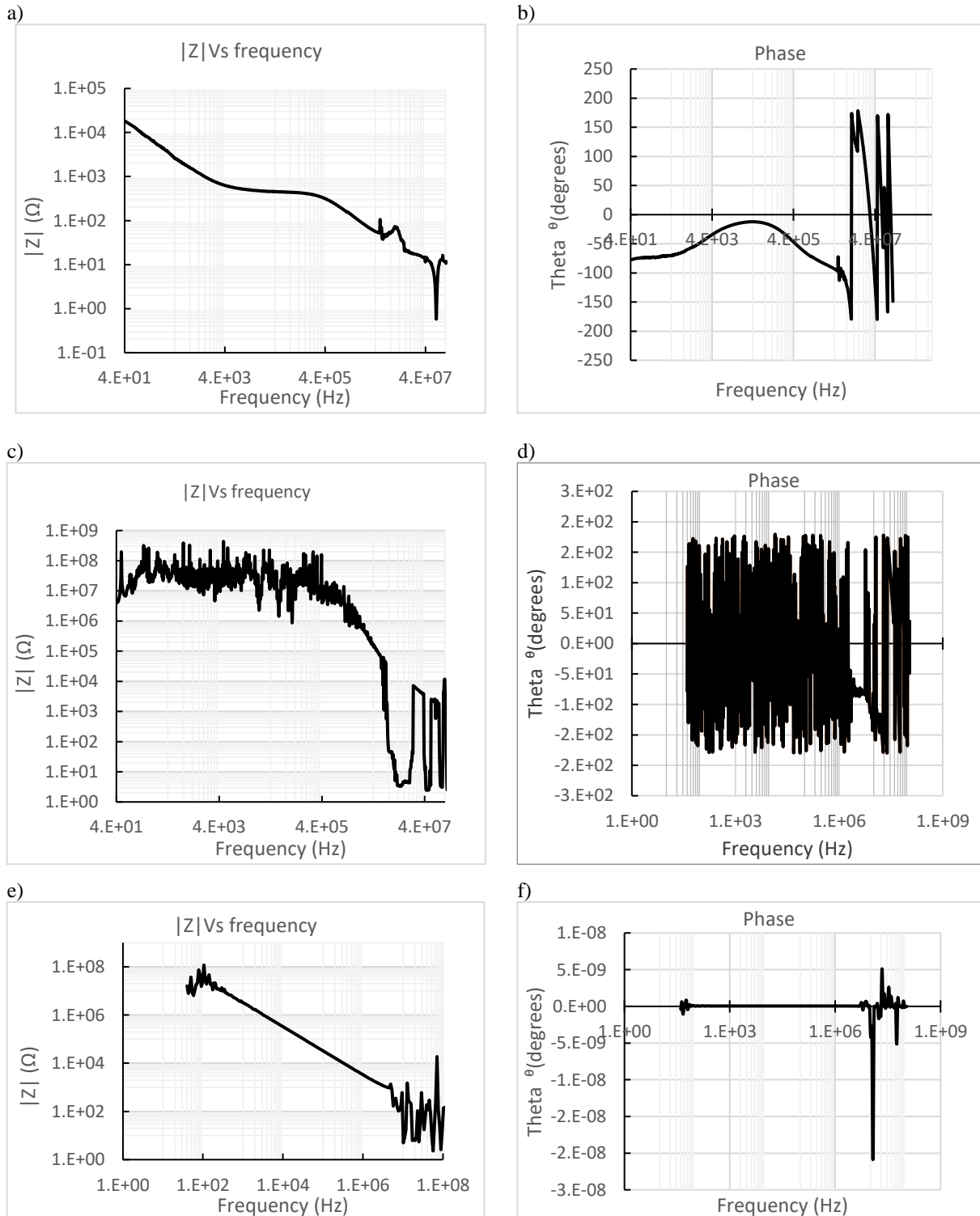
Although the image in Figure 20 and 21 shows promising results according to the literature [2], when we look at results obtained after PCR process in the graphics of Figure 22, the results were not what we would expect. Keeping in mind that the core porpuse of this study was to investigate if there was changes in the impedance related with PCR process. The values presented in Figure 22 are the average of three measurements each cicle more five measurements by Agilent equipment, which perform a total of 150 measurements.

The results shows systematic errors and for this reason we tried to find any visible changes in the obtained graphics.

It was observed small changes in the values (Figure 31 a) and b)) when the device passed through the thermocycling process and the several cycles of the qPCR. Although it seems difficult to assume that these small changes of impedance are consequence of the hybridisation event (Figure 31 c)).

## Annex 10

### Impedance stereoscopy



**Figure 32** Presented above it is the plot of the impedance magnitude with frequency. a) and b) Is the plot of the sample taken when the probes were working and showing results according with the literature. c) and d) It is the plot taken a few days after with same condition and from the plot it is possible to notice that some regions of the graphic were affected. e) and f) Is a teste graphic made with the same parameters but to a SMD capacitor with a fixed value of capacitance 47pF.

Looking through the graphics in the Figure 32 we can see that this problem should be related with the bad shape of the probes used, and in absence of other probes and to keep the same kind of error in all the measurements the Thermocycling process used the same probes and the same method.

## Annex 11

Results obtain form the sample after the UV ozone cleaning and using as electrolyte DI water.

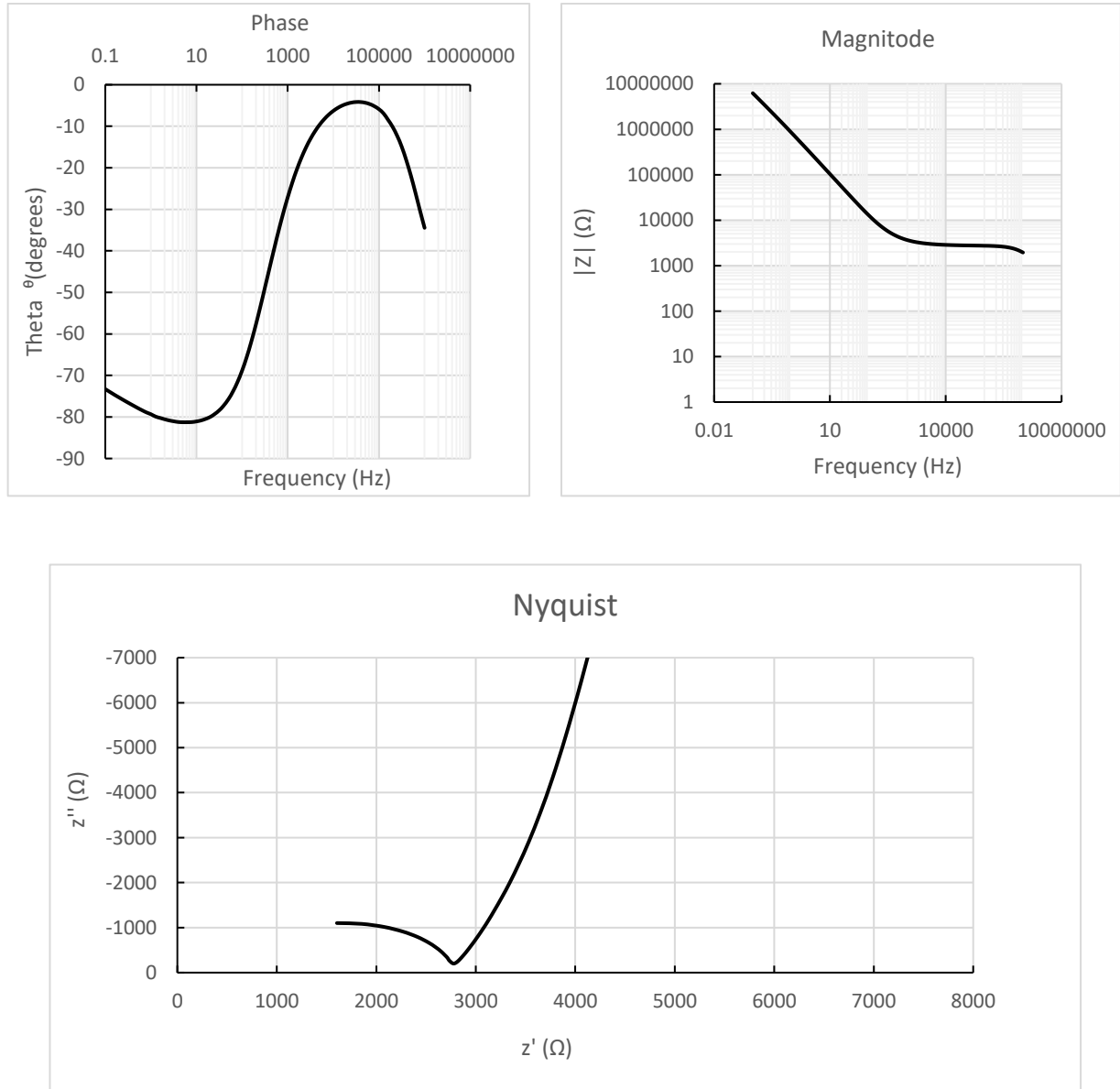


Figure 33 Bode diagram and Nyquist

## Annex 12

### XPS spectroscopy survey spectra

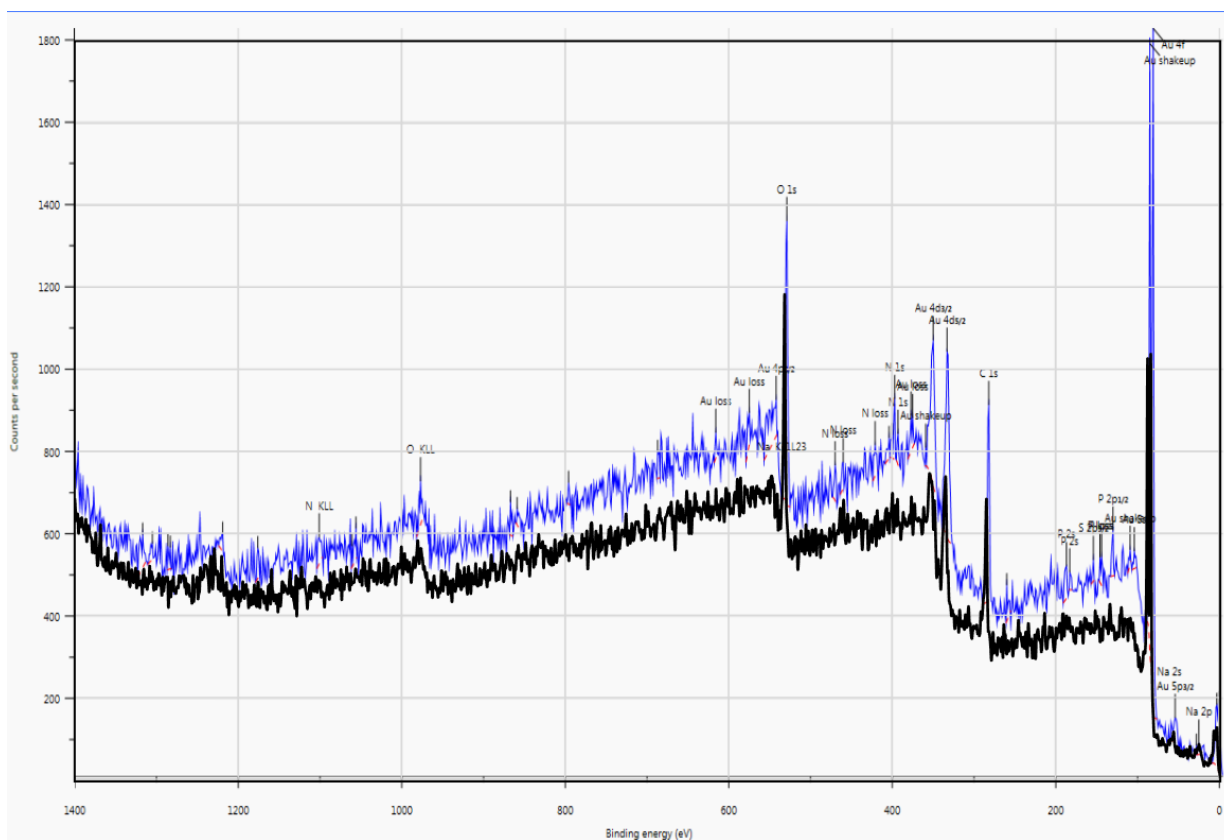


Figure 34 The complete spectrum obtained with XPS